

AD _____

Award Number: W81XWH-09-1-0414

TITLE: Reconstructing the prostate cancer transcriptional
regulatory network

PRINCIPAL INVESTIGATOR: Keyan Salari

CONTRACTING ORGANIZATION: The Leland Stanford Junior University
Stanford, CA 94305

REPORT DATE: July 2010

TYPE OF REPORT: Annual Summary

PREPARED FOR: U.S. Army Medical Research and Materiel Command
Fort Detrick, Maryland 21702-5012

DISTRIBUTION STATEMENT:

⊗ Approved for public release; distribution unlimited

The views, opinions and/or findings contained in this report are those of the author(s) and should not be construed as an official Department of the Army position, policy or decision unless so designated by other documentation.

REPORT DOCUMENTATION PAGE				Form Approved OMB No. 0704-0188	
Public reporting burden for this collection of information is estimated to average 1 hour per response, including the time for reviewing instructions, searching existing data sources, gathering and maintaining the data needed, and completing and reviewing this collection of information. Send comments regarding this burden estimate or any other aspect of this collection of information, including suggestions for reducing this burden to Department of Defense, Washington Headquarters Services, Directorate for Information Operations and Reports (0704-0188), 1215 Jefferson Davis Highway, Suite 1204, Arlington, VA 22202-4302. Respondents should be aware that notwithstanding any other provision of law, no person shall be subject to any penalty for failing to comply with a collection of information if it does not display a currently valid OMB control number. PLEASE DO NOT RETURN YOUR FORM TO THE ABOVE ADDRESS.					
1. REPORT DATE (DD-MM-YYYY) 01-06-2010		2. REPORT TYPE Annual Summary		3. DATES COVERED (From - To) 1 JUN 2009 - 31 MAY 2010	
4. TITLE AND SUBTITLE Reconstructing the prostate cancer transcriptional regulatory network				5a. CONTRACT NUMBER	
				5b. GRANT NUMBER W81XWH-09-1-0414	
				5c. PROGRAM ELEMENT NUMBER	
6. AUTHOR(S) Keyan Salari				5d. PROJECT NUMBER	
				5e. TASK NUMBER	
				5f. WORK UNIT NUMBER	
7. PERFORMING ORGANIZATION NAME(S) AND ADDRESS(ES) The Leland Stanford Junior University, Stanford, CA 94305				8. PERFORMING ORGANIZATION REPORT NUMBER	
9. SPONSORING / MONITORING AGENCY NAME(S) AND ADDRESS(ES) U.S. Army Medical Research and Materiel Command Fort Detrick, Maryland 21702-5012				10. SPONSOR/MONITOR'S ACRONYM(S)	
				11. SPONSOR/MONITOR'S REPORT NUMBER(S)	
12. DISTRIBUTION / AVAILABILITY STATEMENT Approved for public release; distribution unlimited					
13. SUPPLEMENTARY NOTES					
14. ABSTRACT This award has enabled the development of computational methods to analyze and integrate diverse prostate cancer genomic datasets. We have successfully applied one developed method to a prostate cancer dataset, resulting in the identification of genes that may play a causal role in prostate tumor metastasis. Our analysis of prostate tumor DNA copy number data has also uncovered a potentially novel tumor suppressor gene associated with clinically-indolent prostate cancer. This finding may represent a much-needed biomarker capable of distinguishing indolent versus aggressive disease, and may lead to novel strategies for patient management.					
15. SUBJECT TERMS Prostate cancer, genomics, bioinformatics, DNA copy number alteration, gene expression					
16. SECURITY CLASSIFICATION OF:			17. LIMITATION OF ABSTRACT UU	18. NUMBER OF PAGES 36	19a. NAME OF RESPONSIBLE PERSON USAMRMC
a. REPORT U	b. ABSTRACT U	c. THIS PAGE U			19b. TELEPHONE NUMBER (include area code)

Table of Contents

	<u>Page</u>
Introduction.....	4
Body.....	4-5
Key Research Accomplishments.....	6
Reportable Outcomes.....	6
Conclusion.....	6
References.....	7
Appendices.....	7-36

Introduction

Prostate cancer is the most frequently diagnosed cancer among men in the United States; one in six men will be diagnosed in their lifetime, but many of them will not die from their cancer. The observed clinical heterogeneity among prostate cancer patients is likely explained in large part by underlying molecular heterogeneity. DNA copy number alteration (CNA) represents one form of molecular alteration that has been extensively characterized in prostate cancer, and plays a critical role in prostate tumorigenesis via the amplification of oncogenes and deletion of tumor suppressor genes. By altering gene dosage, CNAs not only modify the expression of genes that reside on the affected chromosomal region, but may also aberrantly redirect the transcriptional activity of many other unlinked genes in cases where the region of CNA harbors a transcriptional regulator. In this manner, CNAs perturb the transcriptional regulatory network of prostate tumor cells. An improved understanding of the topology of this network and its most salient nodes might lead to novel diagnostic, prognostic, and therapeutic strategies in the future.

The overall objective of this study is to reconstruct the prostate cancer transcriptional regulatory network and to experimentally validate novel, clinically-relevant regulatory interactions. The hypothesis of this proposal is that CNAs invoke gene expression changes in nearby and distant target genes, and that by using prostate tumor specimens with paired measurements of gene copy number and gene expression, we will be able to detect these CNA-induced gene-expression signatures and infer novel regulatory relationships. The goal of this proposal is to develop and apply a computational method to infer these relationships that collectively form the transcriptional regulatory network of prostate cancer cells.

Body

Year 1 of this award has been dedicated to the collection and processing of multiple prostate cancer genomic datasets, and to the development of computational methods for integrating these datasets. Specifically, two separate approaches to infer relationships between CNAs and gene expression have been developed. The first approach focuses on local or “cis” effects of CNAs; that is, the impact of CNAs on the expression of genes residing in the region of alteration. The second approach focuses on global or “trans” effects of CNAs; that is, the impact of CNAs on the expression of genes residing outside the region of alteration.

Prostate tumor specimens and profiling data. We have generated two large datasets derived from 64 and 90 primary human prostate tumors, respectively, on which to perform integrative genomic analysis. The first series of prostate tumors were profiled for DNA copy number alterations and gene expression changes using Stanford 44K cDNA microarrays [Lapointe et al. PNAS 2004; Lapointe et al. Cancer Research 2007]. The second series of prostate tumors were profiled for DNA copy number alterations using Agilent 44K CGH arrays and for gene expression changes using Stanford Human Exonic Evidence-Based Oligonucleotide (HEEBO) arrays.

Data pre-processing. For each copy number data, background-subtracted log₂-transformed fluorescence ratios have been normalized by median-centering genes on each array. For gene

expression data, background-subtracted log₂-transformed fluorescence ratios have been normalized by median-centering genes for each array and for each gene iteratively. We have included for subsequent analysis those genes measured with high quality (Cy5 or Cy3 channel fluorescence signal intensity at least 1.5-fold above background). Map positions for each probe from the three microarray platforms were mapped to the human genome reference sequence (hg18).

Preliminary data analysis. Statistically significant DNA copy number changes have been identified by Circular Binary Segmentation (CBS) [Olshen et al. 2004] and Fused Lasso [Tibshirani et al. 2008] in each of the two datasets. We also identified regions with recurrent DNA copy number changes across all the tumors using the tool Genomic Identification of Significant Targets in Cancer (GISTIC) [Beroukhi et al. 2007]. These analyses revealed several novel regions of recurrent amplification and deletion in prostate cancer, harboring potential oncogenes and tumor suppressor genes, respectively. Two regions of recurrent deletion on chromosomes 5q21 and 6q15 were identified disproportionately among tumors with a clinically-indolent course of disease. This finding is of interest, as there currently are no good biomarkers of clinically-indolent prostate cancer. Identifying men who need aggressive treatment versus those who could avoid the attendant risks and complications of such treatment is currently a challenge in the clinical management of patients with prostate cancer. We are currently examining this novel region of deletion and functionally validating candidate tumor suppressor genes [Huang et al., in preparation]. This line of investigation ultimately has the potential to yield novel insights into prostate cancer pathobiology as well as point to novel therapeutic and/or risk stratification strategies.

Computational methods development. We have completed development of a method to detect the local or “cis” effects of copy number alterations on gene expression. The method, DNA/RNA-Integrator (DR-Integrator) automates the identification of chromosomal regions with significant amplifications and deletions, and identifies genes with strong correlation in their DNA copy number and gene expression levels [Salari et al. 2010]. DR-Integrator also performs supervised analysis of DNA copy number and gene expression data; that is, given two sample groups of interest (e.g., clinically-indolent vs. clinically-aggressive tumors), DR-Integrator identifies genes with the greatest difference in copy number and expression between the two groups. This type of analysis helps identify specific alterations that might underlie molecular or clinical phenotypes of interest. This method has successfully been applied in a comparative study between copy number and gene expression levels of prostate cancer metastases and primary tumors [Holcomb et al. 2009]. It has also been applied to a study of breast cancer cell lines [Kao et al. PLoS ONE 2009].

Our method to detect global or “trans” effects of copy number alterations on gene expression is in continued development. This method examines the correlations between copy number alterations in one chromosomal region with the gene expression levels of sets of genes on other chromosomes. Because genes that function in the regulation of other genes (e.g., transcription factors and chromatin-modifying factors) are often in regions of copy number alteration, these genetic lesions have the capacity to affect the expression of hundreds to thousands of other genes. The main goal of this method is to identify the most significant of such regulatory relationships in prostate cancer cells.

Key research accomplishments

- Collection and processing of two high-quality prostate tumor datasets profiled for DNA copy number alterations and gene expression levels
- Development of computational method for identification of local or “cis” effects of DNA copy number alteration on gene expression levels
- Identification of novel regions of deletion in clinically-indolent prostate tumors
- Continued development of computation method for identification of global or “trans” effects of DNA copy number alteration on gene expression levels

Reportable outcomes

1. Huang S, **Salari K**, Gulzar ZG, Brooks JD, Pollack JR. Genomic profiling identifies a novel tumor-suppressor deleted in prostate cancer. In preparation.
2. Malhotra S, Lapointe J, Higgins JP, Ferrari M, Montgomery K, **Salari K**, van de Rijn M, Brooks JD, and Pollack JR. A tri-marker proliferation index provides superior prognostic performance in prostate cancer. Submitted.
3. **Salari K**, Tibshirani R, Pollack JR. DR-Integrator: a new analytic tool for integrating DNA copy number and gene expression data. *Bioinformatics*. 2010 Feb 1;26(3):414-6.
4. Holcomb IN, Young JM, Coleman I, **Salari K**, Grove DI, Hsu L, True LD, Roudier MP, Morrissey CM, Higano CS, Nelson PS, Vessella RL, Trask BJ. Comparative analyses of chromosome alterations in soft-tissue metastases within and across patients with castration-resistant prostate cancer. *Cancer Research* 2009 Oct 1;69(19):7793-7802. Epub 2009 Sep 22.
5. Kao J*, **Salari K***, Bocanegra M, Choi YL, Girard L, Gandhi J, Kwei KA, Hernandez-Boussard T, Wang P, Gazdar AF, Minna JD, Pollack JR. Molecular profiling of breast cancer cell lines defines relevant tumor models and provides a resource for cancer gene discovery. *PLoS One*. 2009 Jul 3;4(7):e6146. *Co-first authors.
6. Presentation of DR-Integrator at the AACR-Translating the Cancer Genome Conference, Boston, MA, February 2009.

Conclusion

The support of this award has yielded the development of computational methods to analyze and integrate diverse molecular profiling data. We have successfully applied one developed method to a prostate cancer dataset, resulting in the identification of genes that may play a causal role in prostate tumor metastasis. Our analysis of prostate tumor DNA copy number data has also uncovered a potentially novel tumor suppressor gene associated with clinically-indolent prostate cancer. This finding may represent a much-needed biomarker capable of distinguishing indolent versus aggressive disease, and may lead to novel strategies for patient management. We are continuing to work on a second method for integration of DNA copy number and gene expression data in the second year of this award, and expect further biological insights to be generated by the application of the method to our prostate tumor datasets.

References

Beroukhir R, Getz G, Nghiemphu L, Barretina J, Hsueh T, Linhart D, Vivanco I, Lee JC, Huang JH, Alexander S, Du J, Kau T, Thomas RK, Shah K, Soto H, Perner S, Prensner J, DeBiasi RM, Demichelis F, Hatton C, Rubin MA, Garraway LA, Nelson SF, Liao L, Mischel PS, Cloughesy TF, Meyerson M, Golub TA, Lander ES, Mellinghoff IK, Sellers WR. Assessing the significance of chromosomal aberrations in cancer: methodology and application to glioma. *Proc. Natl Acad. Sci. USA* (2007) 104:20007–20012.

Holcomb IN, Young JM, Coleman I, Salari K, Grove DI, Hsu L, True LD, Roudier MP, Morrissey CM, Higano CS, Nelson PS, Vessella RL, Trask BJ. Comparative analyses of chromosome alterations in soft-tissue metastases within and across patients with castration-resistant prostate cancer. *Cancer Research* 2009 Oct 1;69(19):7793-7802. Epub 2009 Sep 22.

Huang S, Salari K, Gulzar ZG, Brooks JD, Pollack JR. Genomic profiling identifies a novel tumor-suppressor deleted in prostate cancer. In preparation.

Kao J, Salari K, Bocanegra M, Choi YL, Girard L, Gandhi J, Kwei KA, Hernandez-Boussard T, Wang P, Gazdar AF, Minna JD, Pollack JR. Molecular profiling of breast cancer cell lines defines relevant tumor models and provides a resource for cancer gene discovery. *PLoS One*. 2009 Jul 3;4(7):e6146.

Lapointe J, Li C, Higgins JP, van de Rijn M, Bair E, Montgomery K, Ferrari M, Egevad L, Rayford W, Bergerheim U, Ekman P, DeMarzo AM, Tibshirani R, Botstein D, Brown PO, Brooks JD, Pollack JR. Gene expression profiling identifies clinically relevant subtypes of prostate cancer. *Proc Natl Acad Sci USA* 2004 Jan 20; 101(3): 811-16.

Lapointe J, Li C, Giacomini CP, Salari K, Huang S, Wang P, Ferrari M, Hernandez-Boussard T, Brooks JD, Pollack JR. Genomic profiling reveals alternative genetic pathways of prostate tumorigenesis. *Cancer Res.* 2007 Sep 15;67(18):8504-10.

Malhotra S, Lapointe J, Higgins JP, Ferrari M, Montgomery K, Salari K, van de Rijn M, Brooks JD, and Pollack JR. A tri-marker proliferation index provides superior prognostic performance in prostate cancer. Submitted.

Olshen AB, Venkatraman ES, Lucito R, Wigler M. Circular binary segmentation for the analysis of array-based DNA copy number data. *Biostatistics*. 2004 Oct;5(4):557-72.

Tibshirani R, Wang P. Spatial smoothing and hot spot detection for CGH data using the fused lasso. *Biostatistics* (2008) 9:18–29.

Appendices

See attached journal articles.

Gene expression

DR-Integrator: a new analytic tool for integrating DNA copy number and gene expression data

Keyan Salari^{1,2,*}, Robert Tibshirani^{3,4} and Jonathan R. Pollack^{1,*}¹Department of Pathology, ²Department of Genetics, ³Department of Health Research & Policy and⁴Department of Statistics, Stanford University, Stanford, CA, USA

Received on August 5, 2009; revised on November 17, 2009; accepted on December 17, 2009

Advance Access publication December 22, 2009

Associate Editor: David Rocke

ABSTRACT

Summary: DNA copy number alterations (CNA) frequently underlie gene expression changes by increasing or decreasing gene dosage. However, only a subset of genes with altered dosage exhibit concordant changes in gene expression. This subset is likely to be enriched for oncogenes and tumor suppressor genes, and can be identified by integrating these two layers of genome-scale data. We introduce DNA/RNA-Integrator (DR-Integrator), a statistical software tool to perform integrative analyses on paired DNA copy number and gene expression data. DR-Integrator identifies genes with significant correlations between DNA copy number and gene expression, and implements a supervised analysis that captures genes with significant alterations in both DNA copy number and gene expression between two sample classes.

Availability: DR-Integrator is freely available for non-commercial use from the Pollack Lab at <http://pollacklab.stanford.edu/> and can be downloaded as a plug-in application to Microsoft Excel and as a package for the R statistical computing environment. The R package is available under the name 'DRI' at <http://cran.r-project.org/>. An example analysis using DR-Integrator is included as supplemental material.

Contact: ksalari@stanford.edu; pollack1@stanford.edu

Supplementary information: Supplementary data are available at *Bioinformatics* online.

1 INTRODUCTION

DNA microarray technology has been leveraged to make genome-scale measurements across multiple layers of cellular molecules, e.g. gene expression (Schena *et al.*, 1995), DNA copy number (Pinkel *et al.*, 1998; Pollack *et al.*, 1999), protein expression (Haab *et al.*, 2001) and microRNA expression (Calin *et al.*, 2004), among others. While each data type alone provides a unique snapshot of a cell's state, an integrative analysis of two or more complementary data types can reveal much more than the sum of its parts. DNA copy number alterations (CNAs) represent one data layer extensively measured among many tumor types using array-based comparative genomic hybridization (array CGH). CNAs lead to the amplification and deletion of oncogenes and tumor-suppressor genes (TSGs), respectively, and thereby play a critical role in tumorigenesis. While delineating CNAs across many samples facilitates the identification

of oncogenes (in regions of recurrent amplification) and TSGs (in regions of recurrent deletion), cumulatively such genetic changes often span a substantial proportion of the genome, thereby obfuscating the distinction between 'driver' cancer genes selected for by a genetic event and nearby 'passenger' genes incidentally co-amplified or deleted. Similarly, when comparing cancer cells to normal cells, thousands of genes are often differentially expressed, rendering discrimination of the most salient, primary changes from correlated, downstream changes difficult.

One useful approach to aid cancer gene discovery is to integrate DNA copy number and gene expression profiles (Adler *et al.*, 2006; Garraway *et al.*, 2005; Hyman *et al.*, 2002; Pollack *et al.*, 2002). Tumors often harbor CNAs altering the gene dosage of hundreds or thousands of genes. However, due to tissue-specific expression or feedback regulation, among other mechanisms, expression levels of many of these genes may remain unaltered. Because the effects of CNAs are mediated by changes in gene expression, the subset of genes exhibiting concordant changes in both DNA copy number and gene expression (e.g. amplified and over-expressed genes) are likely to be enriched for candidate oncogenes and TSGs.

While several software tools and statistical methods have been developed to analyze DNA copy number data (Beroukhi *et al.*, 2007; Olshen *et al.*, 2004; Tibshirani and Wang, 2008) or gene expression data (Reich *et al.*, 2006; Subramanian *et al.*, 2005; Tusher *et al.*, 2001) separately, few methods have been developed for their integration (Berger *et al.*, 2006; Carrasco *et al.*, 2006; Hautaniemi *et al.*, 2004). In particular, to our knowledge there is no widely available software tool that facilitates multiple integrative analyses with a user-friendly interface. Here, we describe our development of DR-Integrator, a broadly useful package of tools to integrate array CGH and gene expression microarray data for the nomination of candidate cancer genes.

2 FEATURES

The DR-Integrator software package contains two analysis tools: DR-Correlate and DR-SAM.

2.1 Correlation analysis

DR-Correlate aims to identify genes with expression changes explained by underlying CNAs. To that end, this tool performs an analysis to identify all genes with statistically significant correlations between their DNA copy number and gene expression levels. Three

*To whom correspondence should be addressed.

options for the statistic to measure correlation are implemented: (i) Pearson's correlation; (ii) Spearman's rank correlation; and (iii) an 'extremes' *t*-test. For Pearson's and Spearman's correlations, the respective correlation coefficient is computed for each gene. For the extremes *t*-test, a modified Student's *t*-test (Tusher *et al.*, 2001) is computed for each gene, comparing gene expression levels of samples comprising the lowest and the highest quantiles with respect to DNA copy number. In other words, for each gene the samples are rank-ordered by DNA copy number and samples below the lowest quantile and above the highest quantile form two groups whose gene expression is compared with a modified *t*-test. The percentile cutoff defining the two quantile groups is user-adjustable.

2.2 Two-class supervised learning analysis

DNA/RNA-Significance Analysis of Microarrays (DR-SAM) performs a supervised analysis to identify genes with statistically significant differences in both DNA copy number and gene expression between different classes (e.g. tumor subtype-A versus tumor subtype-B). The goal of this analysis is to identify genetic differences (CNAs) that mediate gene expression differences between two groups of interest. DR-SAM implements a modified Student's *t*-test to generate for each gene two *t*-scores assessing differences in DNA copy number (t_{DNA}) and differences in gene expression (t_{RNA}). A final score (S) is computed by first summing the copy number *t*-score and gene expression *t*-score, and then weighting the sum by the ratio of the two *t*-scores ($0 \leq w \leq 1$). The weight is applied to favor genes with strong differences in both DNA copy number and gene expression between the two classes. That is, a gene with statistically equal differences in copy number and in gene expression (i.e. $t_{\text{DNA}} = t_{\text{RNA}}$) will have a weight of 1, while genes with unbalanced contributions from copy number and expression will have a weight less than 1, resulting in a lower score:

$$S = w * (t_{\text{DNA}} + t_{\text{RNA}})$$

$$w = \min \left\{ \frac{t_{\text{DNA}}}{t_{\text{RNA}}}, \frac{t_{\text{RNA}}}{t_{\text{DNA}}} \right\} \quad (1)$$

2.3 False discovery rate estimation

To account for multiple hypothesis testing, both DR-Correlate and DR-SAM calculate a measure of statistical significance called the *q*-value, which is based on the false discovery rate (FDR). This is achieved by randomly permuting the sample labels a large number of times (user-defined; default: 1000 times) to disrupt the correlations between the paired DNA copy number and gene expression measurements. For each random permutation of the data, a test score is computed for every gene. To calculate a gene-specific *q*-value, each observed score is compared to the distribution of random scores and the FDR is estimated as previously described (Storey and Tibshirani, 2003).

2.4 Additional features

DR-Integrator performs several preprocessing steps including smoothing of copy number data, calling significant copy number alterations with the Fused Lasso method (Tibshirani and Wang, 2008), and merging DNA/RNA datasets from different platforms to allow for integrative analyses. DR-Integrator also allows the user to specify the FDR cutoff for an analysis and generate DNA/RNA 'heatmaps' for genes achieving statistical significance. Automatic

imputation of missing expression data, using the nearest neighbor algorithm, is also performed. Finally, we note that DR-Integrator is not limited to the analysis of DNA copy number and gene expression data, but can be used to integrate any paired data types where a 1-to-1 mapping between measured elements can be made. An example analysis is shown on a dataset of DNA copy number and gene expression profiles of 50 breast cancer cell lines (Supplementary Figure S1).

3 IMPLEMENTATION

DR-Integrator has been developed in R and Microsoft Visual Basic v6.5, and runs as a plug-in to Microsoft Excel under the Windows operating system (2000/XP/Vista). With the use of Windows emulators, DR-Integrator can also be run on Mac OS X, Linux and Unix-based operating systems. The statistical methods can also be applied natively in the R interpreter on any of the above platforms.

ACKNOWLEDGEMENTS

The authors would like to thank members of the Pollack Lab for helpful discussions, and Adrienne Pollack for the DR-Integrator logo art.

Funding: National Institutes of Health (CA97139 and CA112016 to J.R.P.); Paul & Daisy Soros Foundation (to K.S.); Medical Scientist Training Program (to K.S.).

Conflict of Interest: none declared.

REFERENCES

- Adler, A.S. *et al.* (2006) Genetic regulators of large-scale transcriptional signatures in cancer. *Nat. Genet.*, **38**, 421–430.
- Berger, J.A. *et al.* (2006) Jointly analyzing gene expression and copy number data in breast cancer using data reduction models. *IEEE/ACM Trans. Comput. Biol. Bioinform.*, **3**, 2–16.
- Beroukhi, R. *et al.* (2007) Assessing the significance of chromosomal aberrations in cancer: methodology and application to glioma. *Proc. Natl Acad. Sci. USA*, **104**, 20007–20012.
- Calin, G.A. *et al.* (2004) MicroRNA profiling reveals distinct signatures in B cell chronic lymphocytic leukemias. *Proc. Natl Acad. Sci. USA*, **101**, 11755–11760.
- Carrasco, D.R. *et al.* (2006) High-resolution genomic profiles define distinct clinico-pathogenetic subgroups of multiple myeloma patients. *Cancer Cell*, **9**, 313–325.
- Garraway, L.A. *et al.* (2005) Integrative genomic analyses identify MITF as a lineage survival oncogene amplified in malignant melanoma. *Nature*, **436**, 117–122.
- Haab, B.B. *et al.* (2001) Protein microarrays for highly parallel detection and quantitation of specific proteins and antibodies in complex solutions. *Genome Biol.*, **2**, RESEARCH0004.
- Hautaniemi, S. *et al.* (2004) A strategy for identifying putative causes of gene expression variation in human cancers. *J. Franklin Inst.*, **341**, 77–88.
- Hyman, E. *et al.* (2002) Impact of DNA amplification on gene expression patterns in breast cancer. *Cancer Res.*, **62**, 6240–6245.
- Olshen, A.B. *et al.* (2004) Circular binary segmentation for the analysis of array-based DNA copy number data. *Biostatistics*, **5**, 557–572.
- Pinkel, D. *et al.* (1998) High resolution analysis of DNA copy number variation using comparative genomic hybridization to microarrays. *Nat. Genet.*, **20**, 207–211.
- Pollack, J.R. *et al.* (1999) Genome-wide analysis of DNA copy-number changes using cDNA microarrays. *Nat. Genet.*, **23**, 41–46.
- Pollack, J.R. *et al.* (2002) Microarray analysis reveals a major direct role of DNA copy number alteration in the transcriptional program of human breast tumors. *Proc. Natl Acad. Sci. USA*, **99**, 12963–12968.
- Reich, M. *et al.* (2006) GenePattern 2.0. *Nat. Genet.*, **38**, 500–501.
- Schena, M. *et al.* (1995) Quantitative monitoring of gene expression patterns with a complementary DNA microarray. *Science*, **270**, 467–470.

Storey,J.D. and Tibshirani,R. (2003) Statistical significance for genomewide studies. *Proc. Natl Acad. Sci. USA*, **100**, 9440–9445.

Subramanian,A. et al. (2005) Gene set enrichment analysis: a knowledge-based approach for interpreting genome-wide expression profiles. *Proc. Natl Acad. Sci. USA*, **102**, 15545–15550.

Tibshirani,R. and Wang,P. (2008) Spatial smoothing and hot spot detection for CGH data using the fused lasso. *Biostatistics*, **9**, 18–29.

Tusher,V.G. et al. (2001) Significance analysis of microarrays applied to the ionizing radiation response. *Proc. Natl Acad. Sci. USA*, **98**, 5116–5121.

Comparative Analyses of Chromosome Alterations in Soft-Tissue Metastases within and across Patients with Castration-Resistant Prostate Cancer

Ilona N. Holcomb,¹ Janet M. Young,¹ Ilisa M. Coleman,¹ Keyan Salari,⁷ Douglas I. Grove,² Li Hsu,² Lawrence D. True,³ Martine P. Roudier,⁴ Colm M. Morrissey,⁵ Celestia S. Higano,⁵ Peter S. Nelson,¹ Robert L. Vessella,^{4,6} and Barbara J. Trask¹

Divisions of ¹Human Biology and ²Public Health Sciences, Fred Hutchinson Cancer Research Center; Departments of ³Genetics, ⁴Urology, and ⁵Medicine (Division of Oncology), University of Washington; and ⁶Veterans Affairs Puget Health Sciences Center, Seattle, Washington; and ⁷Department of Pathology, Stanford University, Stanford, California

Abstract

Androgen deprivation is the mainstay of therapy for progressive prostate cancer. Despite initial and dramatic tumor inhibition, most men eventually fail therapy and die of metastatic castration-resistant (CR) disease. Here, we characterize the profound degree of genomic alteration found in CR tumors using array comparative genomic hybridization (array CGH), gene expression arrays, and fluorescence *in situ* hybridization (FISH). By cluster analysis, we show that the similarity of the genomic profiles from primary and metastatic tumors is driven by the patient. Using data adjusted for this similarity, we identify numerous high-frequency alterations in the CR tumors, such as 8p loss and chromosome 7 and 8q gain. By integrating array CGH and expression array data, we reveal genes whose correlated values suggest they are relevant to prostate cancer biology. We find alterations that are significantly associated with the metastases of specific organ sites, and others with CR tumors versus the tumors of patients with localized prostate cancer not treated with androgen deprivation. Within the high-frequency sites of loss in CR metastases, we find an overrepresentation of genes involved in cellular lipid metabolism, including *PTEN*. Finally, using FISH, we verify the presence of a gene fusion between *TMPRSS2* and *ERG* suggested by chromosome 21 deletions detected by array CGH. We find the fusion in 54% of our CR tumors, and 81% of the fusion-positive tumors contain cells with multiple copies of the fusion. Our investigation lays the foundation for a better understanding of and possible therapeutic targets for CR disease, the poorly responsive and final stage of prostate cancer. [Cancer Res 2009;69(19):7793–802]

Introduction

Genomic analyses of malignant disease are intended to distinguish the molecular features that underlie carcinogenesis and identify clinical targets. Moreover, comparing primary and metastatic tumors is an exceptionally useful way to assess the molecular alterations associated with stage or progression.

The plethora of molecular events that occur in prostate cancer, with no single ubiquitous alteration, illustrate the complex biology

of this disease. This complexity is likely to result, in part, from different genetic backgrounds and environmental exposures of the patients. One way to reduce this heterogeneity when comparing primaries to metastases is to assay both tumor types from the same patient, but these matching sets are difficult to obtain. A decade or more can elapse between the resection of the primary tumor by prostatectomy, detection of overt metastases, and death from castration-resistant (CR) disease. To address this deficiency, we set out to obtain sets of primary and metastatic tumors from the same patient. Although technical limitations prevented us from including bone metastases in this study, we present here analyses of an extraordinary set of multiple soft-tissue metastases.

To block the effects of androgens on tumor growth, patients with advanced disease are often deprived of androgen by surgical or chemical castration. However, aggressive and ultimately lethal CR disease inevitably develops. Few treatment options with clinical benefits exist (1–3), and most represent palliative interventions once this CR state is achieved.

One potential diagnostic marker and treatment target, the fusion of the *TMPRSS2* and *ERG* genes, has generated considerable interest (4–10). Deletion of the 3-Mbp region of 21q22.2 between the promoter of the androgen-regulated serine-protease *TMPRSS2* and the 3' exons of *ERG*, a member of the oncogenic ETS family of transcription factors, is the principal mechanism for this gene fusion (7, 10). Androgens are presumed to drive the expression of this oncogenic fusion, which is found in ~30% of prostate cancers.

Here, we characterize the genomic changes in CR prostate cancer using matching sets of primary prostate tumors and metastases. This work reveals alterations that might have causative properties, clinical value, or site-specific consequences for this end-stage prostate cancer.

Materials and Methods

Sample acquisition. Use of human samples was approved by the Institutional Review Boards of participating institutions. Tumor samples were collected by radical prostatectomy or from autopsies performed at the University of Washington Medical Center under the rapid autopsy program as described previously (11). Available clinical data (stage, Gleason grade, treatment, etc.) are provided in Supplementary Table S1. Autopsies were done within 2 to 4 h of death on 14 patients [median (range) age at death, 67 y (47–83 y)] with clinically diagnosed CR disease. Fifty-four tumors were obtained from various organ sites (Supplementary Table S2). Radical prostatectomy specimens from 19 individuals with organ-confined (i.e., localized) prostate cancer not treated by androgen deprivation were also collected.

Specimens ($n = 73$) were embedded in freezing media (Tissue-Tek OCT Compound, Sakura Finetek) and stored in liquid nitrogen. Cells from the 54 CR tumors, 9 localized prostate cancers (LocPC), or normal stromal of 10

Note: Supplementary data for this article are available at Cancer Research Online (<http://cancerres.aacrjournals.org/>).

Requests for reprints: Barbara J. Trask, Human Biology Division, Fred Hutchinson Cancer Research Center, 1100 Fairview Avenue North, Mail Stop C3-168, PO Box 19024, Seattle, WA 98109. Phone: 206-667-1470; Fax: 206-667-4023; E-mail: btrask@fhcrc.org.
©2009 American Association for Cancer Research.
doi:10.1158/0008-5472.CAN-08-3810

LocPC patients were isolated by laser-capture microdissection (LCM) as described previously (12). A pathologist (L.D.T.) reviewed all LCM images.

DNA isolation and amplification. DNA from LCM-collected samples was isolated using the QIAamp DNA Micro kit (Qiagen, Inc.). DNA from 42 tumors (Supplementary Table S2) was amplified by ligation-mediated PCR (LMP) as described previously (13). DNA samples from 12 CR tumors and 9 LocPC tumors could not successfully be amplified by LMP and instead were amplified using a whole genome amplification (WGA) kit, WGA2 (Sigma-Aldrich). DNAs amplified from these two methods are comparable (14). Of the 10 normal samples, 5 were amplified by LMP and 5 by WGA.

Reference DNA was obtained from the peripheral blood of a single female individual isolated using the QIAamp DNA Blood Mini kit (Qiagen, Inc.). The amplification method for all reference samples was matched with the test sample.

Array comparative genomic hybridization analysis. The bacterial artificial chromosome (BAC) clones that make up the array, array comparative genomic hybridization (array CGH) methods, and analyses have been described previously (14, 15). Clone coordinates given refer to the May 2004 sequence assembly (Build 35).

The \log_2 -ratio array data were normalized with a block-level Loess algorithm (16) and processed by Circular Binary Segmentation (CBS; ref. 17) to organize the output into segments of approximately equal copy number. Thresholds for calling loss and gain in arrays of LMP- or WGA-amplified material were determined using the array results obtained from the normal-cell samples amplified by LMP or WGA, respectively, as described previously (14).

CBS data were subjected to hierarchical/complete linkage clustering (similarity metric was correlation centered) using Gene Cluster software (18). The tree was produced using TreeView.⁸

Significant associations between alterations and tumor state (i.e., CR primaries or CR metastases) or CR organ site (i.e., prostate, lymph-node metastasis, or liver metastasis) were identified using the Significance Analysis of Microarrays (SAM) method (19) using response formats two-class (unpaired) and multiclass, respectively. SAM is based on a modified *t* statistic and uses random permutations of class labels to estimate a false discovery rate (FDR). For each analysis, 1,000 permutations were done.

The methods for gene ontology analyses and tests of statistical significance are as described previously (14, 20).

RNA isolation and amplification. Total RNA from LCM samples was isolated using the Arcturus PicoPure RNA Isolation kit (Molecular Devices) and DNase-treated using the RNase-Free DNase Set (Qiagen, Inc.). The reference RNA was a pool of equal amounts of total RNA isolated from the LNCaP, DU145, PC3, and CWR22 cell lines (American Type Culture Collection). Experimental and reference total RNA samples were subjected to two rounds of amplification using the MessageAmp aRNA kit (Applied Biosystems/Ambion, Inc.).

Expression array analysis. cDNA probe pairs were prepared by amino-allyl reverse transcription using 2 μ g of amplified RNA and labeling with Cy3-dCTP (experimental) or Cy5-dCTP (reference; Amersham Bioscience). Custom microarrays composed of 6,760 cDNA clones selected from the Prostate Expression Database⁹ repository of human prostate expressed sequence tag data were constructed and hybridized as previously described (21).

Combined DNA/RNA analysis. Measurements for genes represented by multiple clones on the Prostate Expression Database expression array were averaged. Each gene expression measurement was paired with a copy-number measurement from the BAC probe nearest to that gene. Correlated data were identified by performing a Pearson's correlation for the CBS-determined BAC clone measurement and gene expression level for each gene. Statistical significance was determined using a Bonferroni correction to adjust for multiple hypothesis testing.

To identify genes with significant differences in both copy number and gene expression between primary and metastatic prostate cancer specimens, the DNA/RNA-SAM (DR-SAM) method of DR-Integrator was

used.¹⁰ Briefly, for each gene, a modified Student's *t* test was applied to generate a copy-number score and a gene-expression score for the primary or metastatic samples. The two scores were summed and weighted to favor genes with substantial differences between the two tumor types. Significance was established by recalculating the scores on 1,000 random permutations of the sample labels (FDR of 5%).

TPRSS2:ERG fluorescence *in situ* hybridization. Five-micrometer tumor sections from frozen tissue blocks were fixed in 3:1 methanol/acetic acid. Four BAC DNAs were used as probes, RP11-35C4 (probe 1), RP11-95I21 (probe 2), RP11-476D17 (probe 3), and RP11-120C17 (probe 4) (Fig. 4). BAC DNA was labeled using a nick-translation kit and either Spectrum Red-dUTP, Spectrum Green-dUTP, or Spectrum Aqua-dUTP (Abbot Molecular). Hybridization was performed as described previously (22).

Fluorescence *in situ* hybridization (FISH) signals were scored manually ($\times 100$ oil immersion). Fusion-positive tumors had positive nuclei (i.e., juxtaposition of probe 1 and probe 3 with concurrent loss or dissociation of probe 2) in at least 20 of 50 cells analyzed. We designated the tumor as possessing multiple copies of the fusion if at least five of 20 positive nuclei showed at least two gene-fusion probe conformations. The results were confirmed in a second FISH experiment (using the same scoring criteria) testing for retention of probe 1 concurrent with dissociation or loss of probe 4.

Results

Hierarchical clustering groups tumors from the same patient together. We performed hierarchical cluster analysis to evaluate relationships among the 54 CR tumors from 14 patients based on their genomic alterations. These CR tumors include those resected from the prostate (and called CR primaries here) and multiple soft-tissue metastatic sites. Tumors most often group with other tumors from the same patient, rather than cluster by organ of origin (Fig. 1A). The tumors for 11 of the 14 ($\sim 79\%$) patients define patient-specific clusters. The closest neighbor in the hierarchy for 53 of 54 tumors is a tumor from the same patient. Including LocPC and normal arrays did not alter the relationships observed for the CR tumors (Fig. 1B). The consistency of alterations for the tumors of a given patient is illustrated in Fig. 1C and emphasized by the separation of the distributions of pairwise correlation coefficients calculated for all intratumor pairs versus for all intertumor pairs (Supplementary Fig. S1).

Tumor-related loci and candidate genes in the frequent alterations of CR tumors. Every position in the genome is represented in the cumulative spectrum of changes observed in one or more of the 54 CR tumors (Fig. 2). To summarize these results, we first adjusted for the variation in number of tumors evaluated for each patient before calculating the frequency of genomic alterations across the CR patients. BAC clones encompassed by a lost or gained segment were assigned a value of -1 or 1 , respectively; no change was assigned a value of 0 . For each loss or gain, we first calculated the average value for each patient and then averaged the resultant fractions across all 14 patients to represent the frequency of a given deviation in this patient set. All frequencies noted in this work are these adjusted frequencies.

To define deviations of interest, we used the one-sample binomial test to calculate a threshold frequency such that for any deviation with frequency exceeding this threshold, the 99% confidence interval of its frequency did not include 0 . This frequency is $z^2/(n + z^2)$, where z is the critical value (Standard normal table) and n is the sample size. For n of 14 and P value of

⁸ <http://rana.lbl.gov/EisenSoftware.htm>

⁹ <http://www.pedb.org>

¹⁰ K. Salari and J. Pollack DNA/RNA-Significance Analysis of Microarrays (DR-SAM). In preparation 2009.

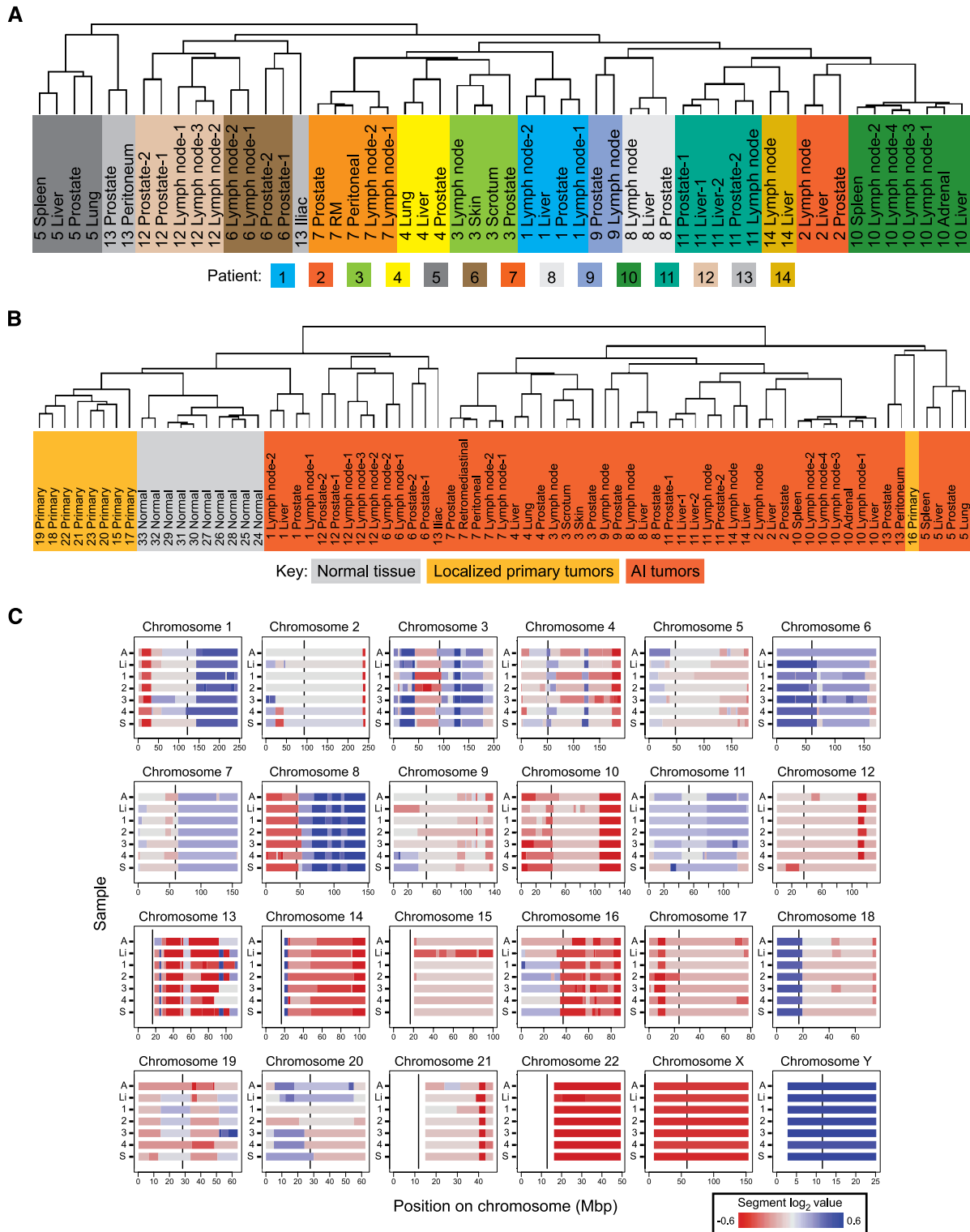


Figure 1. Similarity of the tumors of a given patient. Trees from hierarchical clustering of segmented data from (A) the CR tumors and (B) the CR tumors, LocPCs, and normal prostate stromal tissue. In both trees, the patient number precedes the organ description, and numerical suffixes indicate multiple tumors from the same organ. Each color in A indicates tumors from a different patient; in B, the three sample types are each shaded with a different color. The third panel (C) shows heat maps by chromosome of the CBS segment data for each of the seven tumors from patient 10. Red, negative segment values (regions of copy number loss); blue, positive segment values (regions of copy number gain). Note the expected relative loss of X-chromosome sequences and gain of Y chromosome in this male/female comparison. For each chromosome, the vertical black line within each box indicates centromere position, and the large gaps without data indicate unsurveyed repetitive regions. The Y-axis indicates the sample: A, adrenal metastasis; Li, liver metastasis; 1 to 4, the four lymph-node metastases; and S, spleen metastasis. The color bar below the figure indicates the range of colors representing the segment values shown.

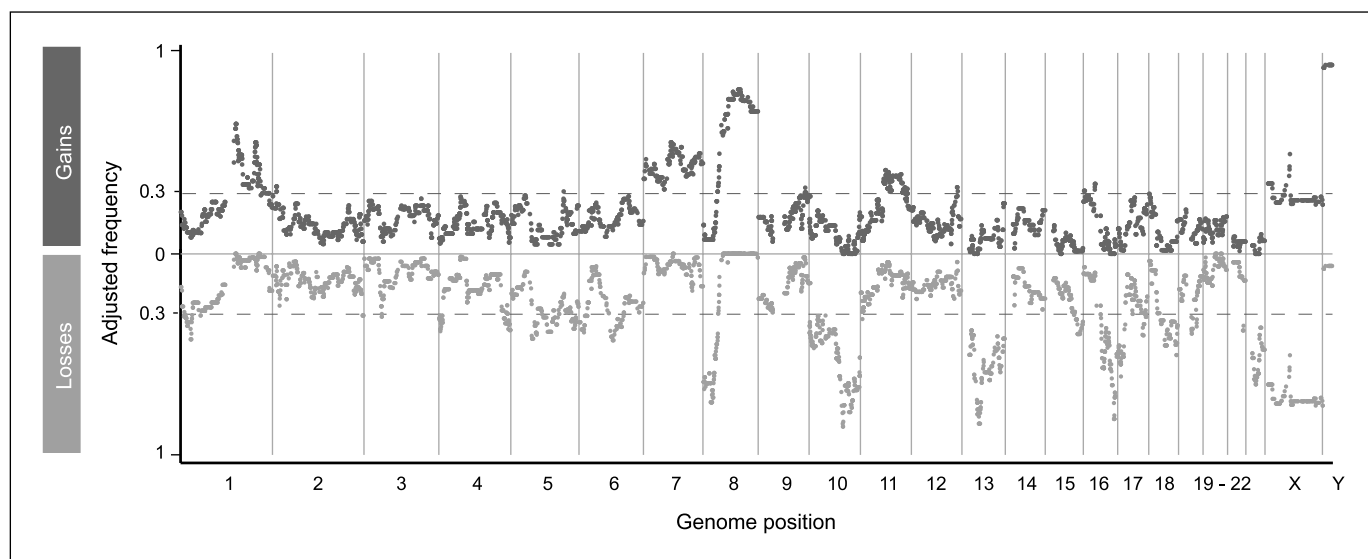


Figure 2. Deviations in CR disease. The Y-axis indicates the adjusted frequency with which each BAC clone on the array was included in a deviant segment across the 54 CR tumors from 14 individuals. The hatched gray lines are drawn at a frequency of 0.3 (i.e., the minimum frequency for significance $P < 0.01$). The X-axis is the genomic position of each BAC clone. Note that loss in X- and gain in Y-chromosome sequences are expected in these male/female comparisons.

<0.01 , i.e., $z = 2.56$, the threshold frequency is ~ 0.3 . The dashed gray lines in Fig. 2 mark this threshold. High-frequency sites of loss or gain exceeding this threshold are listed in Table 1.

Table 1 also provides the locations of the minimally overlapping regions (MOR), which are the most frequently deviant subregions within each set of overlapping deviations. We have identified novel MORs on the two chromosome arms that are thought to play an important role in the biology of prostate cancer, 8p and 8q. Of the four MORs identified for 8p, two have been frequently identified in prostate cancer (23–27), but the more distal MORs in 8p23 have not. We identified four previously reported MORs on 8q (between 8q21.3–q24.22; ref. 23) and three MORs (between 8q11.1–8q21.12) that are heretofore unreported for prostate cancer.

We also examined single BAC clones with extreme \log_2 ratio values (i.e., those in the upper and lower 95th percentile) before smoothing by the CBS method. These singleton deviations, when high, might represent focal sites of gene amplification or, when low, homozygous deletions or loss of multiple copies from polyploid tumor cells. BAC clones whose normalized \log_2 ratio value was outside the 95 percentile in two or more normal control arrays were excluded from this analysis. Supplementary Table S3 lists the singletons identified as deviant in $\geq 30\%$ of the CR tumors (adjusted frequency) and the genes encompassed by them. The BAC clones that overlap sites of normal copy number variation are noted.¹¹ We observed singleton deviations that encompass known cancer-related genes (*AR*, *C13*, *CDH13*, *MMP16*, *MYC*, *PTEN*, and *PTK2*) and androgen-regulated genes (*AR*, *MMP16*, *MYC*, *NDRG1*, and *TSC22D1*).

Genomic profiles of CR tumors and untreated localized primaries are significantly different. To distinguish sites that relate to metastasis or CR disease, we identified those alterations that occur in significantly greater numbers in the CR tumors ($n = 54$) versus the LocPCs ($n = 9$) and vice versa. We found 26 losses

spanning a total of 306 Mbp and 8 gains spanning a total of 255 Mbp that were significantly (Fisher's exact $P < 0.05$) associated with the CR tumors (Table 1). One of the gains encompasses the androgen receptor, an amplification specifically associated with CR disease (28). In the converse analysis, we found only three losses totaling 20 Mbp (5q22.2–q23.1, 11q14.1, and 20q11.23–q13.12) and six gains spanning 69 Mbp (1p36.33–p34.3, 3p21.31–p21.1, 10q21.3–q22.1, 12q13.11–q14.1, 15q15.1–q15.3, and 16q22.1–q22.2) in significantly greater numbers of LocPC than CR tumors.

To verify our findings, we compared our results to a recent survey summarizing 41 CGH studies examining 872 prostate tumors (23). All of the MORs encompassed by the seven alterations that this survey called common ($>10\%$) to primary prostate cancer (loss at 5q15, 6q15, 8p21.3, 13q21.33, 16q22.1, and 18q21.33–22.1 and gain at 8q22.2) were observed in our LocPCs and were in high frequency in our CR tumors ($\geq 30\%$). Of these, our analysis found that the MORs on 16q and 8q were significantly more associated with CR tumors than with LocPCs (Table 1).

Stratification by CR tumor location identifies organ-specific alterations. We stratified the CR tumors to look for differences that might relate to particular states (i.e., CR primaries or CR metastases) or sites (i.e., CR primaries, lymph-node, or liver metastases). We found that the CR primaries possessed significantly fewer gains and losses (average of 14 gains and 18 losses; Student's P values = 0.008 and 0.004, respectively) than the CR metastases (average of 23 gains and 24 losses).

We used SAM (19) to identify alterations with significantly different frequencies between the CR primaries and metastases. Only two alterations were found, both in significantly more metastases, deletions of 10p15.2–10p15.1 (FDR, 0%, 20% of primaries, and 56% of metastases) and 22q12.1–22q12.3 (FDR, 0%, 27% of primaries, and 80% of metastases). These deletions were also found in significantly fewer LocPCs (11% and 33%, respectively) compared with the entire set of CR tumors. Among the genes encompassed by these loci are the tumor suppressors *PRKCC* (10p15.1), *MYO18B* (20q12.1), and *SEZ6L* (20q12.1).

¹¹ <http://hgsv.washington.edu/>

We next asked what differences might exist between the genomic profiles of the CR tumors from the three organ sites that make up 80% of our CR tumors, i.e., prostate ($n = 15$ from 12 patients), lymph node ($n = 19$ from 11 patients), and liver ($n = 9$ from 8 patients). Figure 3A shows the frequencies of alterations for each set. We found that the prostate tumors had significantly fewer gains (average 14; Student's $P = 0.03$ and 0.005 , respectively) and losses (average 18; Student's $P = 0.02$ and 0.04 , respectively) than lymph-node (averages 21 and 22, respectively) or liver (averages 30 and 24, respectively) metastases. Lymph-node metastases had significantly fewer gains (Student's $P = 0.04$) but not losses compared with liver metastases.

Using SAM, we identified five alterations in significantly more liver metastases, three in more lymph-node metastases, and none in the primary tumors (Fig. 3B). The sites for liver metastases were gains at 5q31.2-5q31.3, 5q35.2-5q35.3, 8p11.21, 11q13.2, and 16p13.3. The gain at 8p encompasses a single gene *ANK1*. The sites for lymph-node metastases were gains at 6p21.32-6p21.2 and 6p21.1 and loss at 22q12.1. Among the genes encompassed by the gains were the oncogene *ETV7* (6p21.31) and the tumor-related genes *PTK7* (6p21.1; ref. 29) and *VEGF* (6p21.1; ref. 30).

Merged copy-number and expression results reveal candidate genes. Genomic alterations in cancer can encompass many genes. To identify those that might relate to tumor phenotypes, we integrated our array CGH data with microarray analyses of expression levels. We were able to obtain copy-number and expression data for 51 of our CR tumors.

We identified 131 genes that showed correlated array CGH segment and microarray expression values at a significance level of 0.05 (Supplementary Table S4; tumor-related and androgen-regulated genes are highlighted). Supplementary Fig. S2 illustrates the correlation between copy number and expression for the following eight genes. The gene with the third highest correlation value was *TMPRSS2*. A significant subset of tumors exhibited negative CBS segment values and lower expression ($n = 15$) or positive CBS segment values and higher expression ($n = 19$) of *TMPRSS2*. Other genes identified were the tumor suppressor *retinoblastoma 1* (*RB1*, deleted in 79% of the CR tumors), *MYC binding protein 2* (*MYCBP2*, deleted in 60%), *mucin 1* (*MUC1*, gained in 57%), *PBX1* (gained in 49%), *PARP1* (gained in 33%), *LSM1* (gained in 31%), and *TP53 binding protein 2* (*TP53BP2*, gained in 30%).

To identify genes with significant differences in both copy number and gene expression between primary and metastatic prostate cancer specimens, we used the DNA/RNA-SAMs (DR-SAM) method of DR-Integrator.¹⁰ At an FDR of 5%, we found 19 genes with higher copy number and expression in CR metastases versus CR primaries and 6 with higher copy number and expression in CR primaries versus CR metastases (Supplementary Table S5). Supplementary Fig. S3 illustrates the correlation between selected genes.

Overrepresentation of ontologically related genes in regions frequently altered in CR tumors. To further prioritize possible genes of interest, we looked for overrepresentation of genes of particular gene-ontology categories in regions frequently ($\geq 30\%$, adjusted frequencies) altered in the CR tumors. Lost and gained segments were evaluated separately. Gene ontology categories and genes are given in Supplementary Table S6. The P value "SimPValue" is a statistic that corrects for gene ontology categories that might be overrepresented due to gene clustering. Categories with a SimPValue of >0.05 should be considered with caution.

Cellular lipid metabolism and catabolic process were two of the four categories with genes overrepresented in CR tumor losses. The former category included the tumor suppressors *PTEN* and *WWOX*, and the latter category included *RBX1*, which functions in a complex with the von Hippel-Lindau tumor-suppressor gene. Seven of the genes belonging to gene-ontology categories enriched in regions of loss (*BNIP3*, *ECHS1*, *HDLBP*, *RNF6*, *UBB*, *UBE2L3*, and *USP10*) and two (*AGT* and *PCDHGC3*) belonging to categories enriched in gains were also identified in our analysis of correlated copy-number alterations and expression levels (Supplementary Table S4).

The *TMPRSS2:ERG* gene fusion is prevalent in CR tumors. One MOR, a deletion in 21q22.2-q22.3 was detected in $\sim 40\%$ (22 of 54) of the CR tumors and 50% (7 of 14) of the patients with CR disease and suggested the presence of a fusion of the 5' portion of the *TMPRSS2* gene and the 3' exons of the *ERG* gene (7, 10).

We used FISH to confirm the presence and assess the copy number of the fusion in the cells of our CR tumors. Figure 4 illustrates our FISH strategies. Of the 52 CR tumors for which we could obtain reliable FISH results, 27 (54%) were positive for the *TMPRSS2:ERG* fusion. All tumors from five patients were positive, and eight patients had at least one fusion-positive tumor. All fusions observed were a result of loss of the 5' *ERG* probe (i.e., deletion). All tumors that showed the deletion in 21q22.2-q22.3 by array CGH had consistent FISH results.

We had FISH, array CGH, and microarray expression analysis for 49 CR tumors, of which 25 were fusion-positive. Tumors with correlated negative array CGH and expression values for *TMPRSS2* ($n = 15$) showed a significant association with possession of the fusion (14 of 15) relative to the tumors with any other trend in array CGH and expression values (Fisher's exact $P = 0.00006$). Of the other 11 fusion-positive tumors, 9 showed negative array CGH and positive expression values, and 2 showed positive array CGH and expression values.

Two or more copies of the *TMPRSS2:ERG* fusions were detected by FISH for 22 (42%) of the CR tumors tested. Thus, multiple copies of the fusion were seen in 22 of the 27 fusion-positive tumors (81%), at least one CR tumor from 8 of the 14 patients (57%), the majority of tumors from 3 of the patients (21%), and all of the tumors from 3 of the patients (21%).

Discussion

Genomic alterations within CR tumors might reveal important biological insights into this ultimately lethal stage of prostate cancer. Our cluster analysis shows that CR tumors from a given patient are more similar to each other than they are to tumors from matching organ sites of other patients. These results argue for a monoclonal origin of metastases, consistent with a recent publication by Liu and colleagues (31) who conclude that most, if not all, metastatic prostate cancers have monoclonal origins. As in our study, Liu and colleagues (31) found that metastatic tumors possess genomic profiles that reflect that of the originating tumor cell.

Androgen deprivation also undoubtedly played a part in generating the similarity of tumors of a given patient. Abrogation of androgen, a hormone with profound effects on tumor biology, places a strong selective pressure on the malignant cell population likely increasing the homogeneity of the tumor population. However, this homogenizing force seems insufficient to generate a

Table 1. High-frequency deviations and MORs in CR tumors

A. Losses

Band	Deviation			MOR		CR-associated	
	Start (Mbp)	Size (Mbp)		Start (Mbp)	Size (Mbp)	Start (Mbp)	Size (Mbp)
1p36.23-p35.1	7.2	25.2	36	16.3	3.5	7.2	25.2
			43	26.7	2.5		
1p33-p32.3	48.4	6.8					
2q37.3	238.6	3.7				238.6	3.7
3p21.31	46.3	1.8	31	46.3	0.6	46.3	1.8
4p16.3-p16.1	0.1	10.6	38	2.7	0.3	0.1	4.4
						5.1	5.6
4q33-q34.3	171.7	9.9	35	175.5	3.5	171.7	9.9
4q34.3-q35.2	182.2	8.2	37	184.3	0.9	182.2	5.2
			38	188.0	2.4		
5q11.2-q13.2	55.1	15.9	42	55.3	7.5		
			40	67.8	2.4		
5q14.2-q22.2	81.7	31.0	39	96.0	13.7		
5q23.1-q23.2	115.4	11.8	35	117.6	7.3		
5q34-q35.2	160.7	15.6	37	165.0	6.1	171.3	5.0
6p25.3-p22.3	0.2	21.5	39	12.3	1.2	5.8	9.1
6q13-q22.31	75.2	43.7	43	88.7	5.2		
			36	103.9	9.8		
8p23.3-p11.21	0.3	40.3	67	1.5	1.7		
			66	4.6	1.6		
			74	19.8	3.5		
			71	25.5	1.8		
10p15.3-q26.3	0.2	135.1	39	0.2	0.1	0.2	42.6
			47	9.0	3.3	50.4	25.7
			44	32.4	2.8	79.1	15.7
			42	43.0	1.0	95.9	39.4
			52	72.0	2.4		
			86	89.4	1.2		
			68	98.2	3.7		
			68	103.4	0.4		
			79	105.9	5.0		
			68	121.7	6.9		
11p15.4	4.2	0.3					
13q11-q34	18.4	95.0	50	18.4	4.4	18.4	9.7
			45	27.0	1.1	97.2	16.2
			80	40.6	0.8		
			85	44.6	3.1		
			64	52.1	0.1		
			63	72.4	2.6		
			59	101.3	2.8		
15q24.3-q25.1	75.1	1.9				71.4	13.9
15q25.1-q26.3	78.7	21.3	40	85.4	7.4	86.5	4.1
						96.6	3.4
16q11.2-q24.3	45.3	43.3	57	49.4	5.3	55.0	4.3
			47	63.6	0.2	65.0	2.2
			82	80.7	1.6	82.4	6.2
17p13.3-p11.2	0.1	19.5	51	0.1	0.5	0.1	15.2
			61	7.6	0.3	15.4	4.2
17q24.2-q25.3	64.6	8.9	41	66.1	2.6	64.6	8.9
17q25.3	74.4	1.6				73.8	2.1
18q12.1-q23	28.2	47.9				75.4	0.7
19p12-q13.11	19.9	20.3	40	34.3	2.2		
19q13.2-q13.31	46.1	2.5	36	47.4	0.6	46.1	2.5
21q22.2-q22.3	38.7	4.5	38	38.7	3.0		
22q11.1-q13.33	16.2	33.2	65	24.6	1.6	16.2	8.2
			46	43.4	6.0	26.7	23.2

(Continued on the following page)

Table 1. High-frequency deviations and MORs in CR tumors (Cont'd)

B. Gains										
Deviation			MOR			CR-associated				
Band	Start (Mbp)	Size (Mbp)	(%)	Start (Mbp)	Size (Mbp)	Start (Mbp)	Size (Mbp)			
1p12-q43	120.0	117.7	65	147.9	2.8	153.6	84.3			
			52	155.2	0.7					
			49	157.6	6.9					
			55	200.3	1.9					
			45	209.4	3.0					
1q41-43	215.6	22.1	33	220.4	7.6					
2p25.1	9.6	1.8	33	9.5	1.2					
5q31.3	140.1	0.8								
7p22.3-q36.3	0.1	158.5	47	5.5	0.5	6.4	16.4			
			45	26.8	2.5	27.7	44.2			
			47	62.0	4.0	75.3	23.6			
			55	72.6	2.6	105.6	42.1			
			55	78.9	1.3					
			53	99.1	3.1					
			44	121.3	5.4					
			46	128.7	0.8					
			48	136.2	0.4					
			50	148.2	5.2					
			8p12-q24.3	36.5	109.6	64	43.3	6.0	42.9	103.2
						69	57.2	8.2		
81	79.3	0.5								
82	93.3	6.0								
79	102.3	2.5								
78	115.1	6.5								
73	131.1	2.4								
9q33.2	122.4	1.1								
9q33.2-q33.3	124.3	3.8	33	124.6	1.1					
9q34.11	129.5	0.8								
11q12.1-q24.1	59.4	63.0	42	65.8	1.2	77.5	39.5			
			41	73.5	1.3					
			39	83.8	18.4					
			40	105.3	4.2					
			33	117.8	0.4					
11q23.3-q24.1	119.0	3.4								
11q24.1-q24.2	123.1	2.7	32	123.1	2.3	123.1	2.3			
12q24.31-q24.32	119.8	4.8	33	119.8	2.8					
16p13.3	0.9	2.4								
16p12.1-p11.1	27.6	6.9	35	29.7	4.8					
18p11.32	0.2	2.0								
Xp22.31-p22.12	7.5	11.8								
Xp11.22-q13.1	51.5	16.5	50	65.1	2.8	65.1	2.8			
NOTE: Losses (A) and gains (B) are listed separately. High frequency is defined as observed with an adjusted frequency of ≥30%. The start position, size, and any constituent MORs observed at higher frequency than the larger deviation are given for each deviation. Mbp positions are rounded to nearest 0.1 Mbp. MORs observed at ≥50% are in bold. The start site and size of CR-associated alterations are given.										
Abbreviation: MOR (%), the peak frequency that defines the MOR.										

NOTE: Losses (A) and gains (B) are listed separately. High frequency is defined as observed with an adjusted frequency of $\geq 30\%$. The start position, size, and any constituent MORs observed at higher frequency than the larger deviation are given for each deviation. Mbp positions are rounded to nearest 0.1 Mbp. MORs observed at $\geq 50\%$ are in bold. The start site and size of CR-associated alterations are given. Abbreviation: MOR (%), the peak frequency that defines the MOR.

single CR genomic signature, as the tumor sets are sufficiently distinct to cluster in patient-specific groups. These differences must reflect the uniqueness of each of our CR patients in terms of his genetic risk factors, environmental exposures, history of therapeutic modalities, and chance events.

Across patients, we find a multitude of high-frequency alterations, some encompassing candidate genes that might relate to

prostate cancer, metastases, and CR disease. Within these alterations were several cancer-related genes with correlated DNA and mRNA values, including *RBI*, the earliest recognized tumor suppressor, and *MUC1*, a marker of prostate cancer progression and a novel therapeutic target (32). *PARP1* was also identified; it is involved in DNA repair and inhibitors of it have received considerable attention as novel therapy of breast cancer (33).

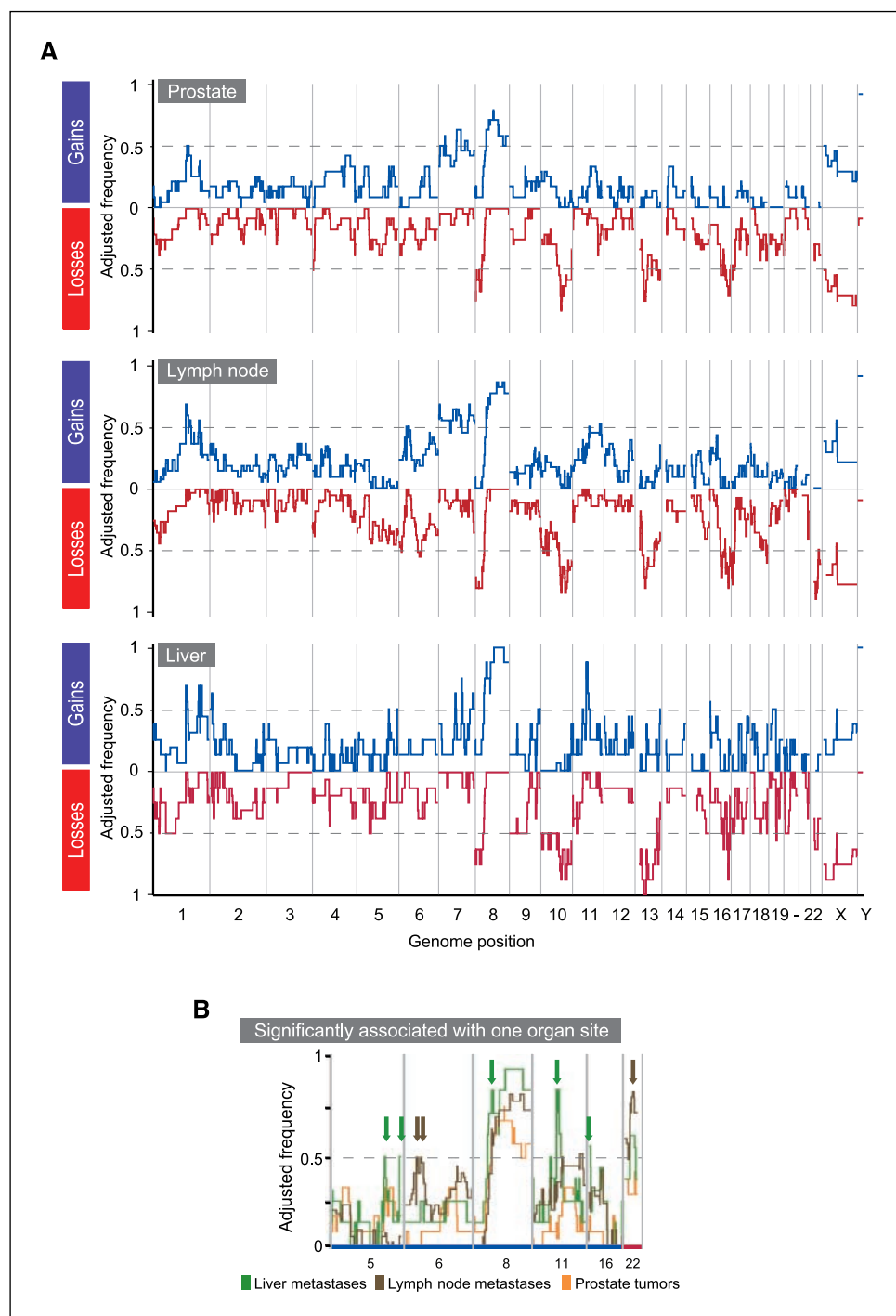


Figure 3. Deviations in CR tumors stratified by organ of origin. *A*, the adjusted frequencies of deviation (*Y*-axis) for gain (blue) or loss (red) for prostate tumors ($n = 15$), lymph-node ($n = 19$), and liver ($n = 9$) metastasis, respectively. Hatched gray lines are drawn at a frequency of 0.5 to aid in graph interpretation. *B*, zoom in for gains on chromosomes 5, 6, 8, 11, and 16 and losses on chromosome 22. Arrows, alterations significantly associated with lymph-node (brown) and liver (green) metastases.

We found that majority of our CR tumors possessed a fusion between *TMPRSS2* and *ERG* as a result of the deletion. The high frequency of CR tumors with multiple copies of the for *TMPRSS2:ERG* fusion is further evidence of the association of amplification of the fusion gene and poor clinical outcome (5). These findings support the idea that it is a promising target for therapeutic interventions (34, 35). Given that the deletion that generates the *TMPRSS2:ERG* fusion was found to encompass the majority of the *TMPRSS2* gene, it was not surprising that we found a significant association between the fusion and negative

array CGH and expression values for *TMPRSS2*. However, a subset of fusion-positive tumors showed higher expression of *TMPRSS2*. This finding may indicate that expression from an intact copy of this androgen-regulated gene might be biologically relevant for some prostate tumors.

Our analysis of high-frequency alterations in CR tumors helps refine prostate cancer-related loci and narrow in on additional candidate genes. No consensus has yet been reached about the critical locus (loci) affected by the two most common alterations seen in prostate cancer, loss at 8p and gain at 8q (28). Our study identifies

four distinct MORs within 8p and seven MORs within 8q. Of the less well-characterized MORs on 8p, one of them encompasses a single gene, *CSMD1*, a candidate suppressor of multiple cancer types (36). *AEG1* (a.k.a. *Lytic* and *MTDH*) is among the genes encompassed by an MOR at 8q21.3-q22.2. *AEG1* is overexpressed in breast, brain, and prostate cancers (37–39) and is thought to promote tumor progression (38–40). The novel MOR at 8q21.12 contains a single gene, *PKIA*, an extremely potent competitive inhibitor of cyclic AMP-dependent protein kinase activity (41). The role of *PKIA* in prostate tumorigenesis merits exploration.

The MORs in our CR data set might help identify other genes relevant to tumorigenesis. The most frequent MOR in our CR tumors was loss at 10q23.31 (86%), which encompasses only *PTEN*, the well-characterized tumor suppressor. Twelve known genes are encompassed by the MOR at 13q14.13-q14.2 (85%), including the *ITM2B* gene, a tumor suppressor (42). Loss at 16q23.3 (82%) encompasses only *CDH13* whose reduced expression in primary prostate tumors is associated with an increased risk of biochemical failure (43). Methylation of *CDH13*, assessed in primary prostate cancer, is generally considered the primary mechanism of gene silencing (44, 45). Our results suggest that methylation in premetastatic states might precede deletion in later stages or that deletion is an alternate mechanism of silencing.

Our gene ontology analysis of the high-frequency alterations in CR tumors also provides insight into candidate genes. The genes that overlapped between our gene ontology analysis and the integration of copy number and expression warrant particular attention. One of these genes encompassed by CR deletion encodes BNIP3, a Bcl-2 family member that can promote apoptosis (46). *RNF6* and *USP10*, which modulate androgen receptor function (47, 48), showed correlated genomic loss and lower expression in a subset of tumors and gain and higher expression in others.

This finding underscores the complexity of the relationship between CR disease and tumor processes controlled by the androgen receptor.

Our analysis of CR tumors provides evidence of accumulation of genomic change with disease progression and outgrowth toward CR disease. We found significantly fewer alterations in CR primaries than in CR metastases and no alterations significantly more associated with CR primaries relative to the matched set of lymph-node and liver metastases. However, we did find eight alterations significantly more associated with those metastatic sites (three and five, respectively). Moreover, we identified several alterations significantly more associated with CR tumors versus LocPCs.

To expand on the significance of our analysis, future work will need to include bone metastasis, a clinically important entity in prostate cancer, and validation of candidate genes. For example, it would be interesting to see the effect of PARP1 inhibitors on models of prostate cancer. The androgen-dependent LNCaP cells and the androgen-independent derivative line (49) would be particularly useful in assessing the role of genes encompassed by CR-associated alterations identified in our study. Direct injection methods for studying prostate cancer cell–bone interactions and the effects that drugs have on these interactions could be used to validate candidate genes and their therapeutic potential (50).

We have shown that CR tumors possess a profound degree of genomic change encompassing many regions that could contain therapeutic targets for metastatic prostate cancer, or at least illuminate the biology of this lethal disease. By combining the results of array CGH and expression microarrays, we have identified numerous candidate regions and genes. Moreover, we have verified that the *TMPRSS2:ERG* fusion, a promising target of cancer therapeutics, is highly prevalent in CR tumors. This extensive and in-depth investigation of the alterations found in

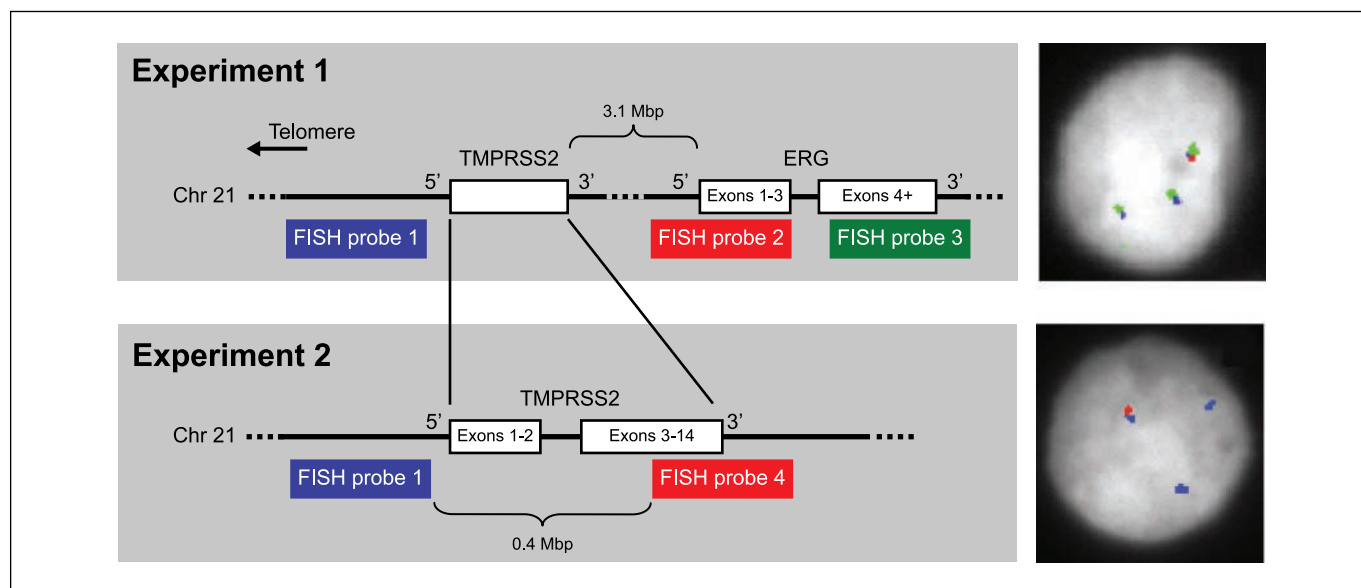


Figure 4. Experimental designs to detect the presence of the *TMPRSS2:ERG* fusion by FISH. In experiment 1, three probes were used to detect the fusion: a probe 5' of *TMPRSS2* (blue, probe 1), one encompassing the 5' exons of *ERG* (red, probe 2), and one encompassing the 3' exons of *ERG* (green, probe 3). In the normal configuration, the signals of all three probes overlap. The fusion is indicated by overlapping signals of probes 1 and 3 with loss or dissociation of probe 2. A CR tumor nucleus with two fusions and one normal probe configuration is shown to the right. In experiment 2, we confirmed the presence of fusion with probe 1 and a second probe encompassing the 3' exons of *TMPRSS2* (red, probe 4) in adjacent tissue sections. Lone probe 1 signals indicate a deletion consistent with a *TMPRSS2:ERG* fusion. Right, a positive nucleus from a section adjacent to the section used to capture the nucleus shown for experiment 1. Gray, 4',6-diamidino-2-phenylindole staining; the hybridization signals are pseudocolored to correspond to the experimental schematics.

CR disease lays the foundation for a better understanding of this final stage of prostate cancer.

Disclosure of Potential Conflicts of Interest

The authors have no potential conflicts of interest.

Acknowledgments

Received 10/3/08; revised 6/11/09; accepted 7/6/09; published OnlineFirst 9/22/09.

References

- Garmey EG, Sartor O, Halabi S, Vogelzang NJ. Second-line chemotherapy for advanced hormone-refractory prostate cancer. *Clin Adv Hematol Oncol* 2008;6:118–22, 27–32.
- Drake CG. Immunotherapy for metastatic prostate cancer. *Urol Oncol* 2008;26:438–44.
- Dreicer R. Current status of cytotoxic chemotherapy in patients with metastatic prostate cancer. *Urol Oncol* 2008;26:426–9.
- Ahlers CM, Figg WD. ETS-TMPRSS2 fusion gene products in prostate cancer. *Cancer Biol Ther* 2006;5:254–5.
- Attard G, Clark J, Ambrosio L, et al. Duplication of the fusion of TMPRSS2 to ERG sequences identifies fatal human prostate cancer. *Oncogene* 2008;27:253–63.
- Mehra R, Tomlins SA, Yu J, et al. Characterization of TMPRSS2-ETS gene aberrations in androgen-independent metastatic prostate cancer. *Cancer Res* 2008;68:3584–90.
- Perner S, Demicheli F, Beroukhi R, et al. TMPRSS2:ERG fusion-associated deletions provide insight into the heterogeneity of prostate cancer. *Cancer Res* 2006;66:8337–41.
- Tomlins SA, Rhodes DR, Perner S, et al. Recurrent fusion of TMPRSS2 and ETS transcription factor genes in prostate cancer. *Science* 2005;310:644–8.
- Tomlins SA, Laxman B, Varambally S, et al. Role of the TMPRSS2-ERG gene fusion in prostate cancer. *Neoplasia* 2008;10:177–88.
- Yoshimoto M, Joshua AM, Chilton-Macneill S, et al. Three-color FISH analysis of TMPRSS2/ERG fusions in prostate cancer indicates that genomic microdeletion of chromosome 21 is associated with rearrangement. *Neoplasia* 2006;8:465–9.
- Morrissey C, True LD, Roudier MP, et al. Differential expression of angiogenesis associated genes in prostate cancer bone, liver and lymph node metastases. *Clin Exp Metastasis* 2008;25:377–88.
- Lin DW, Coleman IM, Hawley S, et al. Influence of surgical manipulation on prostate gene expression: implications for molecular correlates of treatment effects and disease prognosis. *J Clin Oncol* 2006;24:3763–70.
- Klein CA, Schmidt-Kittler O, Schardt JA, Pantel K, Speicher MR, Riethmuller G. Comparative genomic hybridization, loss of heterozygosity, and DNA sequence analysis of single cells. *Proc Natl Acad Sci U S A* 1999;96:4494–9.
- Holcomb IN, Grove DI, Kinnunen M, et al. Genomic alterations indicate tumor origin and varied metastatic potential of disseminated cells from prostate cancer patients. *Cancer Res* 2008;68:5599–608.
- Loo LW, Grove DI, Williams EM, et al. Array comparative genomic hybridization analysis of genomic alterations in breast cancer subtypes. *Cancer Res* 2004;64:8541–9.
- Yang YH, Dudoit S, Luu P, et al. Normalization for cDNA microarray data: a robust composite method addressing single and multiple slide systematic variation. *Nucleic Acids Res* 2002;30:e15.
- Olshen AB, Venkatraman ES, Lucito R, Wigler M. Circular binary segmentation for the analysis of array-based DNA copy number data. *Biostatistics* 2004;5:557–72.
- Eisen MB, Spellman PT, Brown PO, Botstein D. Cluster analysis and display of genome-wide expression patterns. *Proc Natl Acad Sci U S A* 1998;95:14863–8.
- Tusher VG, Tibshirani R, Chu G. Significance analysis of microarrays applied to the ionizing radiation response. *Proc Natl Acad Sci U S A* 2001;98:5116–21.
- Young JM, Endicott RM, Parghi SS, Walker M, Kidd JM, Trask BJ. Extensive copy-number variation of the human olfactory receptor gene family. *Am J Hum Genet* 2008;83:228–42.
- Lin B, Ferguson C, White JT, et al. Prostate-localized and androgen-regulated expression of the membrane-bound serine protease TMPRSS2. *Cancer Res* 1999;59:4180–4.
- Trask BJ. Genome Analysis: A Laboratory Manual. In: *Genome Analysis: A Laboratory Manual*. Vol. 4. Cold Spring Harbor: Cold Spring Harbor Laboratory Press; 1999. p. 303–413.
- Sun J, Liu W, Adams TS, et al. DNA copy number alterations in prostate cancers: a combined analysis of published CGH studies. *Prostate* 2007;67:692–700.
- He WW, Scialovino PJ, Wing J, et al. A novel human prostate-specific, androgen-regulated homeobox gene (NKX3.1) that maps to 8p21, a region frequently deleted in prostate cancer. *Genomics* 1997;43:69–77.
- Dong JT. Chromosomal deletions and tumor suppressor genes in prostate cancer. *Cancer Metastasis Rev* 2001;20:173–93.
- Paris PL, Andaya A, Fridlyand J, et al. Whole genome scanning identifies genotypes associated with recurrence and metastasis in prostate tumors. *Hum Mol Genet* 2004;13:1303–13.
- Perincheri G, Bukurov N, Nakajima K, et al. Loss of two new loci on chromosome 8 (8p23 and 8q12–13) in human prostate cancer. *Int J Oncol* 1999;14:495–500.
- Visakorpi T, Kallioniemi AH, Syvanen AC, et al. Genetic changes in primary and recurrent prostate cancer by comparative genomic hybridization. *Cancer Res* 1995;55:342–7.
- Boudeau J, Miranda-Saavedra D, Barton GJ, Alessi DR. Emerging roles of pseudokinases. *Trends Cell Biol* 2006;16:443–52.
- Ferrara N. VEGF and the quest for tumour angiogenesis factors. *Nat Rev Cancer* 2002;2:795–803.
- Liu W, Laitinen S, Khan S, et al. Copy number analysis indicates monoclonal origin of lethal metastatic prostate cancer. *Nat Med* 2009;15:559–65.
- Li Y, Cozzi PJ. MUC1 is a promising therapeutic target for prostate cancer therapy. *Curr Cancer Drug Targets* 2007;7:259–71.
- Lord CJ, Ashworth A. Targeted therapy for cancer using PARP inhibitors. *Curr Opin Pharmacol* 2008;8:363–9.
- Rubin MA. Targeted therapy of cancer: new roles for pathologists-prostate cancer. *Mod Pathol* 2008;21 Suppl 2:S44–55.
- Bjorkman M, Iljin K, Halonen P, et al. Defining the molecular action of HDAC inhibitors and synergism with androgen deprivation in ERG-positive prostate cancer. *Int J Cancer* 2008;123:2774–81.
- Sun PC, Uppaluri R, Schmidt AP, et al. Transcript map of the 8p23 putative tumor suppressor region. *Genomics* 2001;75:17–25.
- Ash SC, Yang DQ, Britt DE. LYRIC/AEG-1 overexpression modulates BCCIP α protein levels in prostate tumor cells. *Biochem Biophys Res Commun* 2008;371:333–8.
- Emdad L, Sarkar D, Su ZZ, et al. Astrocyte elevated gene-1: recent insights into a novel gene involved in tumor progression, metastasis and neurodegeneration. *Pharmacol Ther* 2007;114:155–70.
- Li J, Zhang N, Song LB, et al. Astrocyte elevated gene-1 is a novel prognostic marker for breast cancer progression and overall patient survival. *Clin Cancer Res* 2008;14:3319–26.
- Emdad L, Sarkar D, Su ZZ, et al. Activation of the nuclear factor κ B pathway by astrocyte elevated gene-1: implications for tumor progression and metastasis. *Cancer Res* 2006;66:1509–16.
- Olsen SR, Uhler MD. Inhibition of protein kinase-A by overexpression of the cloned human protein kinase inhibitor. *Mol Endocrinol* 1991;5:1246–56.
- Latil A, Chene L, Mangin P, Fournier G, Berthon P, Cussenot O. Extensive analysis of the 13q14 region in human prostate tumors: DNA analysis and quantitative expression of genes lying in the interval of deletion. *Prostate* 2003;57:39–50.
- Alumkal JJ, Zhang Z, Humphreys EB, et al. Effect of DNA methylation on identification of aggressive prostate cancer. *Urology* 2008;72:1234–9.
- Esteller M. CpG island hypermethylation and tumor suppressor genes: a booming present, a brighter future. *Oncogene* 2002;21:5427–40.
- Maruyama R, Toyooka S, Toyooka KO, et al. Aberrant promoter methylation profile of prostate cancers and its relationship to clinicopathological features. *Clin Cancer Res* 2002;8:514–9.
- Burton TR, Gibson SB. The role of Bcl-2 family member BNIP3 in cell death and disease: NIPping at the heels of cell death. *Cell Death Differ* 2009;16:515–23.
- Xu K, Shimelis H, Linn DE, et al. Regulation of androgen receptor transcriptional activity and specificity by RNF6-induced ubiquitination. *Cancer Cell* 2009;15:270–82.
- Faus H, Meyer HA, Huber M, Bahr I, Haendler B. The ubiquitin-specific protease USP10 modulates androgen receptor function. *Mol Cell Endocrinol* 2005;245:138–46.
- van Steenbrugge GJ, van Uffelen CJ, Bolt J, Schroder FH. The human prostatic cancer cell line LNCaP and its derived sublines: an *in vitro* model for the study of androgen sensitivity. *J Steroid Biochem Mol Biol* 1991;40:207–14.
- Corey E, Brown LG, Quinn JE, et al. Zoledronic acid exhibits inhibitory effects on osteoblastic and osteolytic metastases of prostate cancer. *Clin Cancer Res* 2003;9:295–306.

Molecular Profiling of Breast Cancer Cell Lines Defines Relevant Tumor Models and Provides a Resource for Cancer Gene Discovery

Jessica Kao^{1,9}, Keyan Salari^{1,2,9}, Melanie Bocanegra¹, Yoon-La Choi^{1,3}, Luc Girard⁴, Jeet Gandhi⁴, Kevin A. Kwei¹, Tina Hernandez-Boussard², Pei Wang⁵, Adi F. Gazdar⁴, John D. Minna⁴, Jonathan R. Pollack^{1*}

1 Department of Pathology, Stanford University, Stanford, California, United States of America, **2** Department of Genetics, Stanford University, Stanford, California, United States of America, **3** Department of Pathology, Samsung Medical Center, Sungkyunkwan University School of Medicine, Seoul, South Korea, **4** Hamon Center for Therapeutic Oncology Research, University of Texas Southwestern Medical Center, Dallas, Texas, United States of America, **5** Division of Public Health Sciences, Fred Hutchinson Cancer Research Center, Seattle, Washington, United States of America

Abstract

Background: Breast cancer cell lines have been used widely to investigate breast cancer pathobiology and new therapies. Breast cancer is a molecularly heterogeneous disease, and it is important to understand how well and which cell lines best model that diversity. In particular, microarray studies have identified molecular subtypes—luminal A, luminal B, ERBB2-associated, basal-like and normal-like—with characteristic gene-expression patterns and underlying DNA copy number alterations (CNAs). Here, we studied a collection of breast cancer cell lines to catalog molecular profiles and to assess their relation to breast cancer subtypes.

Methods: Whole-genome DNA microarrays were used to profile gene expression and CNAs in a collection of 52 widely-used breast cancer cell lines, and comparisons were made to existing profiles of primary breast tumors. Hierarchical clustering was used to identify gene-expression subtypes, and Gene Set Enrichment Analysis (GSEA) to discover biological features of those subtypes. Genomic and transcriptional profiles were integrated to discover within high-amplitude CNAs candidate cancer genes with coordinately altered gene copy number and expression.

Findings: Transcriptional profiling of breast cancer cell lines identified one luminal and two basal-like (A and B) subtypes. Luminal lines displayed an estrogen receptor (ER) signature and resembled luminal-A/B tumors, basal-A lines were associated with ETS-pathway and BRCA1 signatures and resembled basal-like tumors, and basal-B lines displayed mesenchymal and stem/progenitor-cell characteristics. Compared to tumors, cell lines exhibited similar patterns of CNA, but an overall higher complexity of CNA (genetically simple luminal-A tumors were not represented), and only partial conservation of subtype-specific CNAs. We identified 80 high-level DNA amplifications and 13 multi-copy deletions, and the resident genes with concomitantly altered gene-expression, highlighting known and novel candidate breast cancer genes.

Conclusions: Overall, breast cancer cell lines were genetically more complex than tumors, but retained expression patterns with relevance to the luminal-basal subtype distinction. The compendium of molecular profiles defines cell lines suitable for investigations of subtype-specific pathobiology, cancer stem cell biology, biomarkers and therapies, and provides a resource for discovery of new breast cancer genes.

Citation: Kao J, Salari K, Bocanegra M, Choi Y-L, Girard L, et al. (2009) Molecular Profiling of Breast Cancer Cell Lines Defines Relevant Tumor Models and Provides a Resource for Cancer Gene Discovery. PLoS ONE 4(7): e6146. doi:10.1371/journal.pone.0006146

Editor: Mikhail V. Blagosklonny, Roswell Park Cancer Institute, United States of America

Received: March 19, 2009; **Accepted:** June 2, 2009; **Published:** July 3, 2009

Copyright: © 2009 Kao et al. This is an open-access article distributed under the terms of the Creative Commons Attribution License, which permits unrestricted use, distribution, and reproduction in any medium, provided the original author and source are credited.

Funding: This work was supported by grants from the NIH (CA97139; J.R.P.), the California Breast Cancer Research Program, (8KB-0135; J.R.P.), and the Longenbaugh Foundation (J.D.M.). K.S. is a Paul & Daisy Soros Fellow and fellow of the Medical Scientist Training Program. The funders had no role in study design, data collection and analysis, decision to publish, or preparation of the manuscript.

Competing Interests: The authors have declared that no competing interests exist.

* E-mail: pollack1@stanford.edu

⁹ These authors contributed equally to this work.

Introduction

Breast cancer, a leading cause of cancer death in women, is recognized to be a molecularly heterogeneous disease. Markers such as estrogen receptor (ER), progesterone receptor (PR) and ERBB2/HER2 are used for prognostication, and to stratify patients for appropriately targeted therapies [1].

More recently, DNA microarray studies have suggested a refined classification of breast cancer, distinguishing five major subtypes based on different patterns of gene expression, underlying DNA copy number alterations (CNAs), and associated clinical outcomes [2–5]. Luminal subtypes A and B are ER positive and share expression markers with the luminal epithelial layer of cells lining normal breast ducts. Luminal-A tumors are genetically

simple (1q/16p gain) and are associated with favorable outcome, while luminal-B tumors exhibit high proliferation rates, frequent DNA amplification (e.g. 8q24/*MYC*), and less favorable prognosis. Basal-like tumors share expression markers with the underlying basal (myoepithelial) layer of normal breast ducts, are ER negative, exhibit frequent chromosome segmental gains/losses, and are associated with poor outcome in most studies. The *ERBB2* subtype is associated with expression of genes co-amplified with *ERBB2* (encoding HER2) on chromosome cytoband 17q12, and the normal-like subtype shares expression patterns with normal breast tissue.

Breast cancer cell lines have been used widely to investigate breast cancer pathobiology, and to screen and characterize new therapeutics [6,7]. Advantages of cell lines include the relative ease of pharmacologic and genetic manipulation, the variety of available functional assays, and, for some studies, the purity of the cancerous epithelial population (and absence of stromal cell contamination). However, while some investigators choose particular cell lines based on the known ER or HER2 status, many others rely on standard “workhorses” like MCF7 without regard to the particular tumor subtypes being modeled. The recent recognition of microarray molecular subtypes points to the need for additional consideration in cell line selection.

The goal of our study was to profile gene expression and CNAs genome-wide in a collection of 52 publicly-available and commonly-used breast cancer cell lines, in order to assess the relation of these cell lines to the recognized molecular subtypes of breast cancer, and to discover new candidate breast cancer genes and pathways.

Materials and Methods

Breast Cancer Cell Lines

184A1, BT20, BT474, BT483, BT549, Hs578T, hTERT-HME1, MCF7, MCF10A, MDA-MB134, MDA-MB157, MDA-MB175, MDA-MB231, MDA-MB361, MDA-MB436, MDA-MB453, MDA-MB468, SKBR3, T47D, UACC812, UACC893, ZR75-1 and ZR75-30 were obtained from ATCC (Manassas, VA, USA). EFM19 and EFM192A were obtained from DSMZ (Braunschweig, Germany). HCC38, HCC70, HCC202, HCC712, HCC1007, HCC1143, HCC1395, HCC1419, HCC1428, HCC1500, HCC1569, HCC1599, HCC1806, HCC1937, HCC1954, HCC2157, HCC2185, HCC2218, HCC2688 and HCC3153 were obtained from the cell repository of the Hamon Center for Therapeutic Oncology Research, UT Southwestern Medical Center (many are now available from ATCC). CAL51 was a kind gift from J. Gioanni from the Centre Antoine-Lacassagne, Nice, France. SUM44PE, SUM52PE, SUM102PT, SUM149PT and SUM190PT were kind gifts from Dr. Stephen P. Ethier (now available from Asterand, Detroit, MI). MCF10A was grown in MEGM media (Cambrex, East Rutherford, NJ). SUM52PE and SUM149PT were grown in Ham's F12 media with 5% FBS, supplemented with 5 µg/ml insulin and 1 µg/ml hydrocortisone. SUM44PE, SUM102PT and SUM190PT were grown in Ham's F12 with 0.1% BSA, supplemented with 5 µg/ml insulin, 1 µg/ml of hydrocortisone, 5 mM ethanolamine, 10 mM HEPES, 5 µg/ml transferrin, 10 nM of Triiodo Thyronin (T3) and 50 nM sodium selenite (10 ng/ml EGF was also included for SUM102PT). All other cell lines were grown in RPMI-1640 with 10% FBS and 1% Pen/Strep. Clinicopathological characteristics of cell lines are summarized in Table 1. A subset of cell lines (focused on the HCC series) was subjected to a more detailed molecular pathological

characterization of *ESR1*, *PGR*, *ERBB2*, *EGFR* and *BRCA1*, as summarized in Table 2.

RNA and DNA isolation

Cells were grown to 70–80% confluence, then harvested for total RNA and genomic DNA. For HCC lines, RNA was prepared using the Qiagen RNeasy Midi Kit (Qiagen, Valencia, CA) and DNA by phenol/chloroform extraction. For all other lines, RNA was isolated using Trizol (Invitrogen, Carlsbad, CA) according to the manufacturer's protocol, and DNA using the Blood Cell Maxi Kit (Qiagen).

ERBB2 copy number assessment by quantitative PCR

ERBB2 copy number was quantified by real-time quantitative PCR (Q-PCR), using the Chromo4 PCR System (Bio-Rad Laboratories, Hercules, CA). *GAST*, located at 17q21 (on the same chromosomal arm as *ERBB2*) was used as a reference control. PCR primer sequences for *ERBB2* and *GAST* are as follows (forward and reverse, respectively): *ERBB2* (5'-TTGGGAGCCTGGCATTCT-3' and 5'-AGGTCATCG-TGCCCACTCTT-3'); *GAST* (5'-GTAGGCATCCTTCCCC-CATT-3' and 5'-AGCCATGGTCCCTGCTTCTT-3'), with PCR product lengths of 59 and 70 base pairs, respectively. Primers were chosen by TaqMan Primer Express™ 1.5 (Applied Biosystem, Foster City, CA) and purchased from Invitrogen. PCR reactions were carried out in a final volume of 20 µl containing 20 ng genomic DNA, 300 nM each primer (for both *ERBB2* and *GAST*, in independent reactions) and 1× Power SYBR Green PCR Master Mix (Applied Biosystems, Foster City, CA). PCR conditions were as follows: one cycle at 95°C for 10 minutes, followed by 40 cycles each at 95°C for 15 seconds and 60°C for 1 minute. Samples were analyzed in triplicate. Each amplification reaction was checked for the absence of nonspecific PCR products by melting curve analysis. *ERBB2* copy number calculation was carried out using the comparative Ct method [8] after validating that the efficiencies of PCR reactions of both *ERBB2* and *GAST* were equal. Human Genomic DNA (DNA20) (EMD Biosciences, Darmstadt, Germany), a mixture of pooled human whole blood from 6–8 individual male and female donors, was run in every assay as a calibrator sample. *ERBB2* gene copy number in normal human genomic DNA was set as 2 and copy number more than 4 in cell lines was considered to be increased.

mRNA levels of *ESR1*, *PGR*, *ERBB2* and *EGFR*

Transcript levels of *ESR1*, *PGR*, *ERBB2* and *EGFR* were analyzed as a part of RT2 Profiler Custom PCR Array (SuperArray Bioscience, Frederick, MD). After making cDNA from 1.0 µg total RNA using RT2 PCR Array First Strand Kit (SuperArray Bioscience), quantitative PCR was performed with the Chromo4 PCR System (Bio-Rad Laboratories) using RT2 Real-Time SYBR Green PCR Master Mix (SuperArray Bioscience) according to the manufacturer's protocol. We chose two different housekeeping genes, β-actin (*ACTB*) and glyceraldehyde-3-phosphate dehydrogenase (*GAPDH*) as internal controls, using the average of their Ct values. Primers were chosen by Taqman Primer Express™ 1.5 and purchased from Invitrogen, as follows: (forward and reverse, respectively): *ESR1* (5'-ATCTCG-GTTCGCGCATGATGAATCTGC-3' and 5'-TGCTGGACA-GAAATGTGTACACTCCAGA-3'); *PGR* (5'-CCTGTGGG-AGCTGTAAGGTCTT-3' and 5'-GCAGTCATTTCCTTCCA-GCACATA-3'), *ERBB2* (5'-TGACCTGCTGGAAAAGGGG-GAGCG-3' and 5'-TCCCTGGCCATGCGGGAGAATTCA-G-3'); *EGFR* (5'-ATAGTCGCCCAAAGTTCGGTGAGT-3'

Table 1. Clinicopathological features of breast cancer cell lines.

Cell line	Subtype [#]	ER [*]	PR [*]	ERBB2/ HER2 [*]	Source [€]	Tumor type [€]
184A1	B	—	NA	—	RM	NA
BT20	A	—	—	—	PT	AC
BT474	L	+	+	+	PT	IDC
BT483	L	+	+	—	PT	IDC
BT549	B	—	—	—	PT	IDC
CAL51	B	—	NA	—	PE	AC
EFM19	L	+	+	—	PE	IDC
EFM192A	L	+	+	+	PE	AC
HCC38	B	—	—	—	PT	DC
HCC70	A	—	—	—	PT	DC
HCC202	L	—	—	+	PT	DC
HCC712	L	+	—	—	PT	DC
HCC1007	L	+	—	+	PT	DC
HCC1143	A	—	—	—	PT	DC
HCC1187	A	—	—	—	PT	DC
HCC1395	B	—	—	—	PT	DC
HCC1419	L	—	—	+	PT	DC
HCC1428	L	+	+	—	PE	Met AC
HCC1500	L	+	+	—	PT	DC
HCC1569	A	—	—	+	PT	Met C
HCC1599	A	—	—	—	PT	DC
HCC1806	NA	—	—	—	PT	Sq C
HCC1937	A	—	—	—	PT	DC
HCC1954	A	—	—	+	PT	DC
HCC2157	A	—	—	—	PT	NA
HCC2185	L	—	—	—	PE	Met LC
HCC2218	L	—	—	+	PT	DC
HCC2688	L	—	NA	—	PT	DC
HCC3153	A	—	—	—	PT	DC
HS578T	B	—	—	—	PT	C Sar
hTERT-HME1	B	—	NA	—	RM	NA
MCF7	L	+	+	—	PE	Met AC
MCF10A	B	—	—	—	RM	F
MDA134	L	+	—	—	PE	IDC
MDA157	B	—	—	—	PE	Med C
MDA175	L	+	—	—	PE	IDC
MDA231	B	—	—	—	PE	Met AC
MDA361	L	+	+	+	BR	Met AC
MDA436	B	—	—	—	PE	AC
MDA453	L	—	—	+	PE	Met C
MDA468	A	—	—	—	PE	Met AC
SKBR3	L	—	—	+	PE	AC
SUM44	NA	+	+	+	PE	ILC
SUM52	L	+	—	+	PE	Met C
SUM102	B	—	—	—	PE	IDC, apocrine
SUM149	B	—	—	—	PE	Inf
SUM190	L	—	—	+	PT	Inf

Table 1. Cont.

Cell line	Subtype [#]	ER [*]	PR [*]	ERBB2/ HER2 [*]	Source [€]	Tumor type [€]
T47D	L	+	+	—	PE	IDC
UACC812	L	+	—	+	PT	IDC
UACC893	L	—	—	+	PT	IDC
ZR75-1	L	+	—	—	AF	IDC
ZR75-30	L	+	—	+	AF	IDC

Abbreviations: A = Basal A subtype; AC = adenocarcinoma; AF = ascites fluid; B = Basal B subtype; BR = brain; C Sar = carcinoma sarcoma; DC = ductal carcinoma; F = fibrocystic disease; IDC = invasive ductal carcinoma; Inf = inflammatory carcinoma; ILC = invasive lobular carcinoma; L = Luminal subtype; Med C = medullary carcinoma; Met AC = metastatic adenocarcinoma; Met C = metastatic carcinoma; Met LC = metastatic lobular carcinoma; NA = not available; PE = pleural effusion; PT = primary tumor; RM = reduction mammoplasty; Sq C = Squamous Carcinoma.

[#]Determined from this study.

^{*}Determined from the ATCC (<http://www.atcc.org>) and DSMZ (<http://www.dsmz.de>) websites, and references therein, or from this study.

[€]Determined from the ATCC and DSMZ websites, and references therein.

[†]ERBB2 amplified but not highly expressed.

doi:10.1371/journal.pone.0006146.t001

and 5'-ACCACGTCGTCCATGTCTTCTTCA-3'); *ACTB* (5'-GGCTGTGCTGTGGAAGCTAAG-3' and 5'-ATGATG-GAGTTGAAGGTAGTTTCGT-3') [9]. We also analyzed the values of NC11 (normal lymphocyte) cell line for *ESR1*, *PGR*, *ERBB2* and *EGFR* mRNA expression, and the tumor cell values were reported relative to NC11. For data analysis, the comparative Ct method [8] was used.

Western blot analysis and immunohistochemistry (IHC)

Preparation of total cell lysates and Western blotting were done as described previously [10]. Primary antibodies used were mouse monoclonal anti-ER- α (Cell Signaling, Beverly, MA), mouse monoclonal PR (6A1) (Cell Signaling), mouse monoclonal anti-HER2 (Cell Signaling), rabbit monoclonal anti-EGFR (Cell Signaling) and mouse monoclonal anti-actin (Sigma-Aldrich). Actin levels were used as a control for protein loading. Peroxidase-labeled anti-mouse or anti-rabbit antibodies (Amersham Pharmacia, Piscataway, NJ) were used as secondary antibody. IHC on breast cancer cell lines was described previously [11].

BRCA1 mutation analysis

DNA sequence analysis was performed on the entire *BRCA1* gene in available lymphocyte DNA matched to breast cancer cell lines. In the lymphocyte DNA matching HCC3153, a heterozygous duplication of 10 base pairs was detected at position 943 in exon 11 of *BRCA1* (943ins10). The region of *BRCA1* exon 11 containing the 943ins10 mutation was amplified from genomic DNA in the tumor cell line (HCC3153) using standard PCR conditions. Sequence analysis revealed only the mutant sequence. Absence of the normal allele was also confirmed by single strand conformation analysis as well as gel electrophoresis of the amplified fragment on 5% acrylamide denaturing gels.

Gene expression profiling

Gene expression profiling was performed on Human Exonic Evidence Based oligonucleotide (HEEBO) arrays obtained from the Stanford Functional Genomics Facility and containing 36,192

Table 2. Molecular pathological analysis of breast cancer cell line subset.

Cell line	Phenotype	BRCA1	Q-PCR# ERBB2	Q-RT-PCR*				IHC			Western			
				ESR1	PGR	ERBB2	EGFR	ESR1	PGR	ERBB2	ESR1	PGR	ERBB2	EGFR
HCC38	Triple neg		1.18	—	—	—	—	—	—	—	—	—	—	—
HCC70	Triple neg		0.37	—	—	—	+	—	—	—	—	—	—	+
HCC202	ERBB2 amp		28.88	—	—	+	+	—	—	+	—	—	+	+
HCC712	Hormone+		0.95	+	—	—	—	+	+	—	+	—	—	—
HCC1143	Triple neg		1.08	—	—	—	+	—	—	—	—	—	—	+
HCC1187	Triple neg		0.42	—	—	—	—	—	—	—	—	—	—	+
HCC1395	Triple neg		0.36	—	—	—	—	—	—	—	—	—	—	—
HCC1419	ERBB2 amp		8.39	—	—	+	—	—	—	+	—	—	+	—
HCC1428	Hormone+		0.20	+	+	—	—	+	+	—	+	+	—	—
HCC1500	Hormone+		0.38	+	+	—	—	+	+	—	+	—	—	—
HCC1569	ERBB2 amp		33.75	—	—	+	+	—	—	+	—	—	+	+
HCC1806	Triple neg		0.08	—	—	—	+	—	—	—	—	—	—	+
HCC1937	Triple neg	INS C 5382	0.33	—	—	—	+	—	—	—	—	—	—	+
HCC1954	ERBB2 amp		45.01	—	—	+	+	—	—	+	—	—	+	+
HCC2185	Triple neg		0.63	—	—	—	+	—	—	—	—	—	—	+
HCC3153	Triple neg	943 ins 10	0.64	—	—	—	+	—	—	—	—	—	—	+
MCF7	Hormone+		0.56	+	—	—	—	—	—	—	+	—	—	—
BT483	Hormone+		0.19	+	+	—	—	—	—	—	+	+	—	—
BT549	Triple neg		0.63	—	—	—	+	—	—	—	—	—	—	+
MDA157	Triple neg		0.76	—	—	—	+	—	—	—	—	—	—	—
MDA231	Triple neg		0.90	—	—	—	+	—	—	—	—	—	—	+
MDA453	Triple neg		3.88	—	—	+	—	—	—	—	—	—	—	—
MDA134	Hormone+		0.76	+	—	—	—	—	—	—	+	—	—	—
MDA175	Triple neg		0.57	—	—	—	—	—	—	—	—	—	—	—
HMEC1585	Control		0.54	—	—	—	+	—	—	—	—	—	—	+
CALU3	Control		12.59	—	—	+	+	—	—	—	—	—	+	+
NC11	Control		1.75	—	—	—	—	—	—	—	—	—	—	—
DNA20	Control		2.00	—	—	—	—	—	—	—	—	—	—	—

#Gene copy number determined using DNA20 (from normal lymphocytes) as a diploid control; bold values indicate amplification.

*mRNA expression quantified in comparison to the immortalized breast line HMEC1585; Calu3 was used a positive control for *ERBB2*, and MCF7 for *ESR1*.

doi:10.1371/journal.pone.0006146.t002

oligonucleotides representing 18,141 mapped human genes. 40 µg of sample RNA and 40 µg of “universal” reference RNA (derived from 11 different established human cell lines) were differentially labeled with Cy5 and Cy3, respectively, using an amino-allyl coupling protocol, then cohybridized onto the microarray in a high volume mixing hybridization at 65°C for 40 hrs. Details of the array processing and sample labeling/hybridization methods have been described [12]. Following hybridization, arrays were washed and scanned using a GenePix 4000B Axon scanner (Axon Instruments, Union City, CA). Fluorescence ratios were extracted using Spot Reader software (Niles Scientific, Portola Valley, CA) and uploaded to the Stanford Microarray Database [13] for storage, retrieval, and analysis. For two lines, HCC1806 and SUM44PE, expression profiling array hybridizations did not meet quality-control inspection and were excluded from analysis. The complete microarray expression data are available at the Stanford Microarray Database (SMD) (<http://smd.stanford.edu>) and at the Gene Expression Omnibus (GEO) (accession GSE15376); all microarray data reported in the manuscript are described in accordance with MIAME guidelines.

Gene expression profiling analysis

Background-subtracted fluorescence log₂ ratios were globally normalized for each array, and then mean-centered for each gene (i.e. reporting relative to the average log ratio across all samples). Unless otherwise specified, we included for subsequent analysis only well-measured genes defined as those with fluorescence intensities in the Cy5 or Cy3 channel at least 1.5-fold above background in at least 60% of samples. For unsupervised hierarchical clustering, we included only the 8,750 well-measured genes whose expression varied at least 3-fold from the mean in at least 5 samples (Table S1). Hierarchical clustering was performed and displayed using Cluster and TreeView software (<http://rana.lbl.gov/EisenSoftware.htm>). Enrichment for functionally related genes was tested across a collection of 1,687 curated gene sets (C2) using Gene Set Enrichment analysis (GSEA; Release 2.0) [14]. Cell lines were classified according to breast tumor subtype (luminal-A, luminal-B, ERBB2, basal-like and normal-like) using the nearest centroid method applied to the set of “intrinsic genes” (i.e. genes with small within-specimen compared to between-specimen expression variance), as done previously [15], here using

Euclidean distance. To classify breast tumors (from the Sorlie *et al.* dataset [3]) according to cell line subtype (luminal, basal A, or basal B), we first built a classifier by combining the top 100 genes positively and negatively correlating with each of the three “one *vs.* others” cell line subtype distinctions, using Significance Analysis of Microarrays (SAM) [16]. The cell line subtype classifier, comprising 484 genes, was then applied to classify primary tumors using the nearest centroid method (with Euclidean distance). We also classified each cell line as being associated with a good or bad prognosis signature (70-gene prognostic signature [17]), the presence or absence of a wound healing signature (512-gene wound signature [18]), and the presence or absence of an hypoxia signature (123-gene hypoxia signature [19]). For each signature, we calculated the gene expression centroid of the two groups of breast tumors (as determined in the original publications), and then correlated each centroid with cell line expression of the respective signature genes. Membership was assigned to the group with the highest correlation (Pearson correlation).

Array-based comparative genomic hybridization (aCGH)

Arrays for CGH were obtained from the Stanford Functional Genomics Facility. aCGH was performed using cDNA arrays containing 39,632 cDNAs, representing 22,279 mapped human genes (18,049 UniGene clusters [20], together with 4,230 additional mapped ESTs not assigned to UniGene IDs), according to previously published protocols [21,22]. Briefly, 4 μ g of genomic DNA from cell lines was random-primer labeled with Cy5 and co-hybridized onto a microarray along with 4 μ g of Cy3 labeled normal leukocyte female reference DNA. Following overnight hybridization, the arrays were washed and scanned as above. The complete aCGH data are available at SMD and at GEO (accession GSE15376).

aCGH analysis

Background-subtracted \log_2 fluorescence ratios were normalized for each array by mean centering. Well-measured genes used for subsequent analysis were those with fluorescence intensities in the Cy3 reference channel at least 1.4 fold above background. Map positions for arrayed cDNA clones were assigned using the NCBI genome assembly, accessed through the UCSC genome browser database (NCBI Build 36.1). For genes represented by multiple arrayed cDNAs, the average \log_2 ratio was used. The complete processed aCGH dataset is available as Table S2. DNA gains and losses were identified using the cghFlasso (R package for Fused Lasso) method [23], which controls the false discovery rate (FDR) by using normal-normal hybridization arrays to approximate the null distribution of the test statistics (see [23] for more details). A FDR < 1% was used to call gains and losses. The fraction of the genome altered was determined by calculating the fraction of genes with fluorescence ratios ≥ 3 (for amplifications) or with significant non-zero fused lasso calls (for gains and losses). Some analyses (where indicated) were carried out on cytobands (boundaries defined by NCBI Build 36.1) rather than individual genes. For each cell line, cytobands exhibiting CNA were defined as those with at least two genes called by cghFlasso, and the magnitude of the CNA defined as the average \log_2 ratio of genes within the cytoband. We defined high-level DNA amplifications and multi-copy deletions as continuous regions identified by cghFlasso with at least 50% of genes having fluorescence ratios ≥ 3 or ≤ 0.25 respectively. These sites were also checked against known copy number variants (CNVs) reported in the Database of Genomic Variants (<http://projects.tcag.ca/variation>). Significant associa-

tions between cytobands and gene-expression subtypes were identified using SAM with a FDR < 5%.

Integrating genomic and transcriptional profiles

To integrate DNA copy number data (generated using cDNA microarrays) and gene-expression data (HEEBO oligonucleotide arrays), each gene expression measurement was first assigned a DNA copy number from either a probe interrogating the same named gene, or the average copy number of the nearest 5' and 3' probes (NCBI Build 36.1). Identification of genes with correlated copy number and expression was carried out using the DR-Correlate application of DR-Integrator (K. Salari, manuscript in preparation). Briefly, for each gene a modified Student's *t*-test was performed comparing gene expression levels in cell lines from the lowest and the highest deciles of all cell lines' copy number for the same gene; random permutations of sample labels were used to estimate a FDR.

Results

Transcriptional profiling identifies three breast cancer cell line subtypes

To catalog molecular variation in a collection of 52 widely-used breast cancer cell lines, we first profiled gene expression using whole genome oligonucleotide microarrays. Unsupervised hierarchical clustering of the 8,750 most variably expressed genes stratified cell lines into two main groups (see dendrogram, Fig. 1B). One group, designated “luminal” (blue dendrogram branches), contained all the ER-positive cell lines (Fig. 2A), and was characterized by the expression of ER α -regulated genes (e.g. *MYB*, *RET*, *EGR3*, *TFF1*; Fig. 1H, and not shown) [24–27], as well as genes associated with luminal epithelial differentiation (e.g. *GATA3* and *FOXA1*, Fig. 1I) [28].

The other group, designated “basal”, contained only ER-negative cell lines (Fig. 2A) and was characterized by the expression of basal epithelial gene markers including *MSN*, *ETS1*, *CAV1* and *EGFR* (Fig. 1E, and not shown) [29–32]. Basal cell lines were further stratified into two subgroups, designated A and B (in line with Neve *et al.* [33], discussed further below). The basal-A subtype (red dendrogram branches) contained many of the “HCC” lines established at UT Southwestern, including two known *BRCA1* mutant lines (HCC1937, HCC3153) ([34], and this study). Basal-A lines were characterized by expression of *PROM1* (aka CD133), a marker of various cancer stem cells [35], as well as other genes like *GABRP* and *ITCNI* (Fig. 1F and 2C). Some of the basal-A lines also shared expression of luminal epithelial markers like *KRT8* and *KRT18* (Fig. 1G).

The basal-B subtype (orange dendrogram branches) included non-tumorigenic lines (MCF10A, hTERT-HME1, 184A1) as well as several highly invasive lines exhibiting features of epithelial-mesenchymal transition (EMT) (MDA-MB231, MDA-MB436, MDA-MB157, Hs578t) [36]. Basal-B lines were characterized by markers associated with aggressive tumor features, including *PLAT* (plasminogen activator) [37] and *TGFB1* [38] (Fig. 1C), as well as marker phenotypes associated with normal breast and breast cancer progenitor/stem cells (*MUC*[−]/*CALLA*⁺; *CD44*⁺/*CD24*^{−/low}; and *ITGB3*(*CD61*)⁺) (Fig. 2C) [39–41]. In contrast to other basal lines, the subset of mesenchymal-like basal-B lines lacked expression of basal cytokeratin markers *KRT5* and *KRT17* (Fig. 1D, and not shown).

Subtype-specific differences in gene expression could also be identified by pathway analysis, using Gene Set Enrichment Analysis (GSEA) [14]. Included among the top signature associations (Table 3), the luminal cell line subtype was

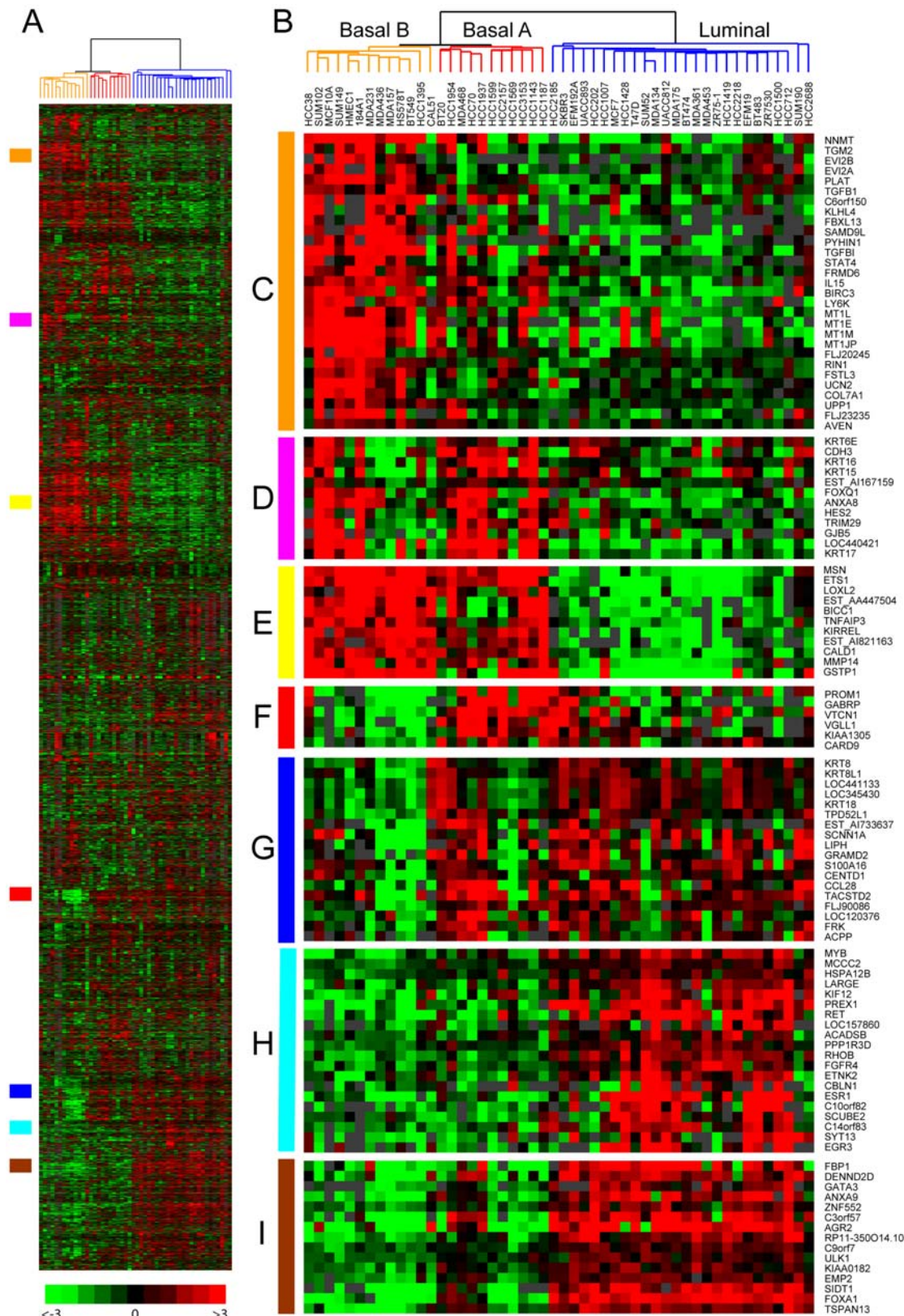


Figure 1. Clustering of expression profiles defines breast cancer cell line subtypes. (A) Thumbnail “heatmap” of two-way hierarchical clustering of 50 breast cancer cell lines (columns) and 8,750 variably expressed genes (rows) (data available as Table S1). Gene expression ratios are depicted by \log_2 pseudocolor scale shown; gray represents poorly measured data. (B) Enlarged view of the sample dendrogram. Clustering stratifies cell lines into two main groups, luminal (blue dendrogram branches) and basal, the latter further subdivided into two subgroups, basal A (red) and basal B (orange). (C–I) Selected gene expression patterns extracted from the cluster; corresponding locations in the thumbnail are indicated by the vertical colored bars. (C) Basal-B; (D) Basal cytokeratins; (E) Basal; (F) Basal-A; (G) Luminal cytokeratins; (H) ER-associated; (I) Luminal differentiation. doi:10.1371/journal.pone.0006146.g001

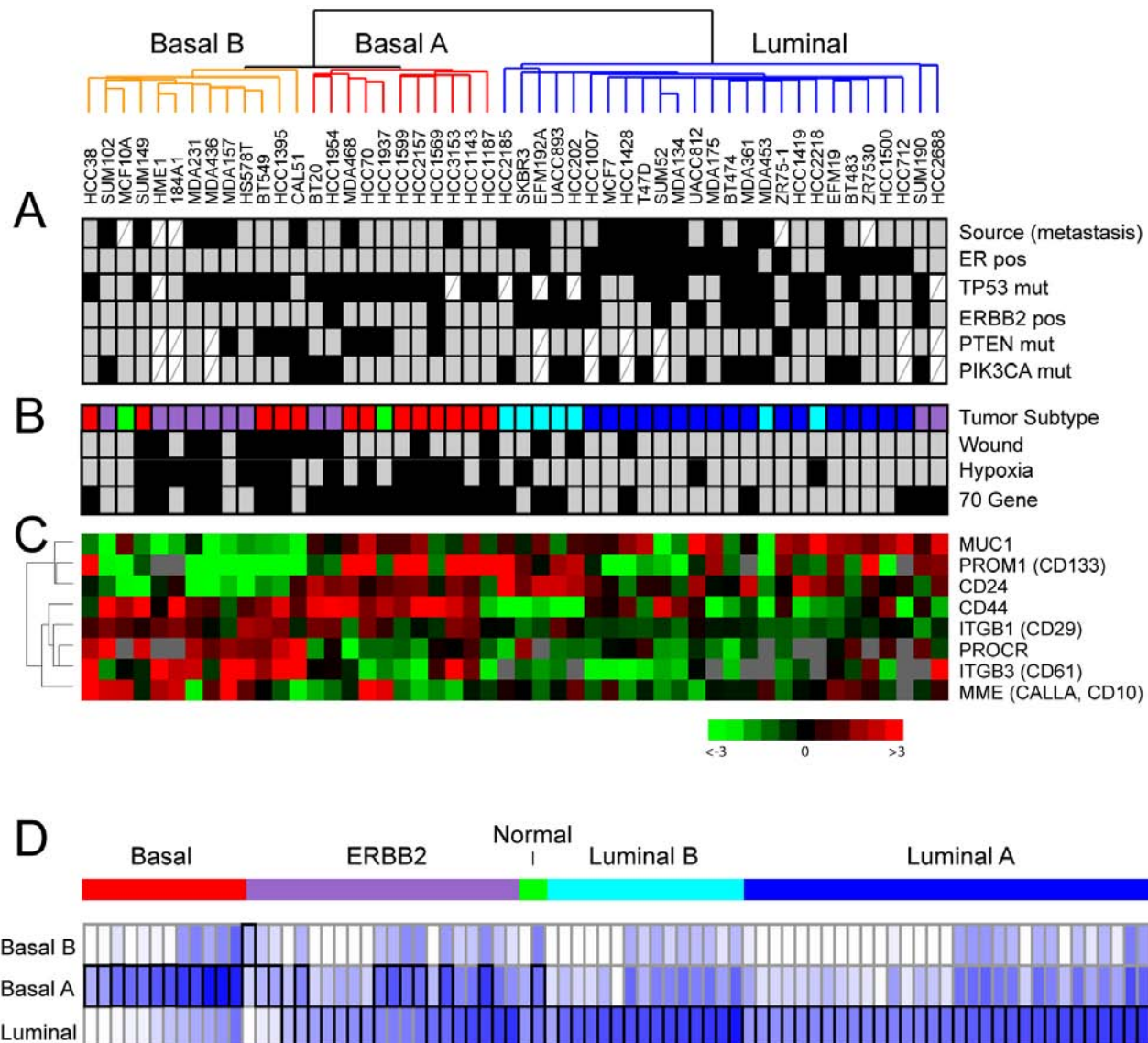


Figure 2. Subtype-specific expression and molecular characteristics. (A) Clinical, pathological and molecular characteristics of cell line expression subtypes. Black boxes indicate metastasis derivation, ER-positivity, *TP53* mutation, *ERBB2*/HER2 positivity, *PTEN* mutation, *PIK3CA* mutation. Mutation data compiled from the Sanger (<http://www.sanger.ac.uk>) and IARC (<http://www-p53.iarc.fr>) websites, and from refs. [94,95]. White cross-hatched boxes indicate missing data. (B) Classification of cell lines by nearest resemblance to tumor gene-expression subtype: luminal A (dark blue), luminal B (light blue), ERBB2-associated (purple), basal-like (red) or normal-like (green); and by positivity (black boxes) for 70-gene, wound and hypoxia signature. (C) Expression levels of selected stem/progenitor cell relevant markers; \log_2 ratios are depicted by pseudocolor scale shown (gray represents poorly measured data). (D) Relation of tumor subtypes to cell line subtypes. Subtype of 86 tumors [3] is shown color-coded as above. Resemblance to each cell line subtype is depicted by Euclidian distance, indicated by blue intensity (representing shorter distances); best match is bracketed in black.

doi:10.1371/journal.pone.0006146.g002

characterized by enriched expression of ER and good prognosis signatures, basal-A by ETS pathway and BRCA1 signatures, and basal-B by EMT and epidermal growth factor (EGF) signatures.

In regard to molecular markers and gene mutations (Fig. 2A), the luminal subtype included all the ER-positive cancer lines ($P < 0.001$, 2-tailed Fisher's exact test), and all but two of the ERBB2-positive lines ($P = 0.002$), half of which were also ER-positive. *PTEN* inactivating mutations and *PIK3CA* activating mutations, functioning on the same pathway, were mutually exclusive in all but one sample. Interestingly, *PTEN* mutations were more common in the combined basal-like cell lines ($P = 0.020$), while *PIK3CA* mutations were more frequent in

luminal lines ($P = 0.022$). *TP53* mutations occurred more often in basal-like lines ($P = 0.038$).

Relationship of breast cancer cell line and tumor subtypes

To determine the relation between breast cancer cell line subtypes (luminal, basal-A, basal-B) and breast tumor subtypes (luminal-A, luminal-B, ERBB2, basal-like, and normal-like), we first classified cell lines according to tumor subtype using a nearest centroid approach applied to the set of "intrinsic genes" used originally to define the tumor subtypes [2,3] (see Methods) (Fig. 2B). By expression patterns, most of the luminal lines most

Table 3. GSEA of breast cancer cell line subtypes.

Subtype	Gene Set	Description	Source	FDR*
Luminal	BRCA_ER_POS	Correlated with ER+ in breast cancer	[17]	0.017
	BRCA_PROGNOSIS_POS	Correlated with good prognosis in breast cancer		0.094
Basal-A	ETSPATHWAY	ETS transcription factor pathway	BioCarta	0.063
	BRCA_BRCA1_POS	Correlated with BRCA1 (germline) in breast cancer	[17]	0.063
	IFN_ALL_UP	Upregulated with interferon- α,β,γ treatment	[96]	0.071
	IFNALPHA_HCC_UP	Upregulated with interferon- α treatment	[97]	0.076
	GLYCOGEN	Glycogen processing	Broad Institute	0.078
Basal-B	JECHLINGER_EMT_UP	Upregulated in EMT	[98]	0.040
	EGF_HDMEC_UP	Upregulated with EGF treatment	[99]	0.042
	DORSEY_DOXYCYCLINE_UP	Upregulated with GAB2 expression	[100]	0.047
	HTERT_DN	Downregulated with hTERT-immortalization	[101]	0.048
	HINATA_NFKB_UP	Upregulated by NF- κ B	[102]	0.049

*Only top five significant gene sets shown.
doi:10.1371/journal.pone.0006146.t003

closely resembled either luminal-A or luminal-B tumors. Most basal-A lines resembled basal-like tumors, and most basal-B lines resembled either basal-like or ERBB2 tumors (despite that none were ERBB2-positive).

We also carried out the reverse analysis, building a cell line subtype classifier to classify 86 breast tumors (from the original Stanford/Norway study defining the five tumor subtypes [3]) according to cell line subtype (see Methods) (Fig. 2D). Notably, all basal-like tumors most resembled basal-A cell lines. Luminal-A and -B tumors most resembled luminal cell lines, while ERBB2 subgroup tumors most resembled either luminal or basal-A cell lines. A similar analysis of breast tumors arising in carriers of *BRCA1* mutation, analyzed from a different dataset (The Netherlands Cancer Institute) [17], revealed highest resemblance in 17 of 18 cases to basal-A lines (not shown), while two *BRCA2* mutation associated cases most resembled luminal cell lines.

In addition to the above cluster-derived luminal/basal tumor subtypes, alternative breast tumor subtype classifiers have been proposed, including a 70-gene prognostic signature supervised on the metastatic/non-metastatic distinction [17], a “wound” signature trained on the serum response of cultured fibroblasts [18], and a hypoxia signature derived from the hypoxic response of cultured mammary and renal tubular epithelial cells [19]. Each of the three signatures predicts unfavorable clinical outcome. Interestingly, the basal-like lines (considered together) were those predominantly expressing the 70-gene ($P=0.001$, Fisher’s exact test) wound ($P=0.004$), and hypoxia ($P<0.001$) signatures (Fig. 2B).

Genomic profiles of breast cancer cell lines

To survey DNA copy number alterations in the panel of 52 breast cancer cell lines, we carried out CGH on cDNA microarrays with validated performance characteristics [21] and covering 22,000 genes with an average mapping resolution (inter-probe distance) of <70 Kb. Across the sample set, the most frequent CNAs (called by cghFlasso—see Methods) were gains on 1q, 3q, 5p, 7p, 8q, 11q, 17q, and 20q, and losses on 3p, 4, 8p, 9p, 11q, 13q, 18p, and Xq.

Overall, the spectrum of cytoband gains and losses was similar in the cell lines compared to primary tumors (Fig. 3A), though the frequency of those CNAs was generally higher with the cell lines. Cell line subtype-specific CNAs could be identified by SAM

analysis (Fig. 3B). Luminal cell lines were characterized by more frequent gains on 1q, 8q, 11q, 12q, 14q, 17q and 20q, and losses on 8p, 9p, 11q, 13q, and 18p. Of these, gains on 1q, 8q, and 20q, and losses on 1p, 8p and 13q (asterisked in Fig. 3B) also characterize luminal-B breast tumors, while 17q gain characterizes ERBB2-associated tumors [4,5]. Notably, simple patterns characteristic of luminal-A tumors (1q+, 16p+, 16q−) were not well-represented among the luminal cell lines. Basal-A and basal-B cell lines also exhibited characteristic gains/losses (Fig. 2B), but none also selectively characteristic of basal-like tumors.

Luminal cell lines displayed overall higher frequencies of high-level DNA amplification (i.e. fluorescence ratios ≥ 3 , corresponding to at least 5-fold amplification [21]) (Fig. 4A), a characteristic shared with luminal-B tumors [4]. Luminal and basal-A lines both exhibited overall higher frequencies of gain/loss (a characteristic feature of basal-like tumors [4]), compared to basal-B lines (Fig. 4B).

Integrated analysis for cancer gene discovery

The molecular profiles generated provide opportunities to identify breast cancer cell lines with an altered copy number and expression of known cancer genes, useful to model pathogenesis and therapy, and to discovery new breast cancer genes. For the latter, high-amplitude CNAs, i.e. high-level DNA amplifications and homozygous deletions, are particularly informative in pinpointing new cancer genes. Within the aCGH dataset we identified 80 loci of high-level amplification in 35 different cell lines, each spanning 49–49,014 Kb (median 1,115 Kb). We also identified 13 multi-copy (possibly homozygous) deletions (fluorescence ratios ≤ 0.25) in 8 cell lines spanning 132–7,825 Kb (median 1,477 Kb). The boundaries of amplicons/deletions did not correspond to known germline CNVs (reported in the Database of Genomic Variants), and, for the subset of recurrent alterations, finding distinct boundaries in different cell lines was more consistent with somatic alteration. Several regions of high-level amplification contained known oncogenes, like 8q24 (*MYC*), 11q13 (*CCND1*) and 17q12 (*ERBB2*). Other amplicons did not correspond to known oncogenes and presumably harbor novel breast cancer genes.

Gains and losses contribute to breast cancer by the increased and decreased expression of oncogenes and tumor suppressors, respectively. Using DR-Correlate (see Methods), we identified 3,511 genes (~18% of all well-measured genes) whose altered

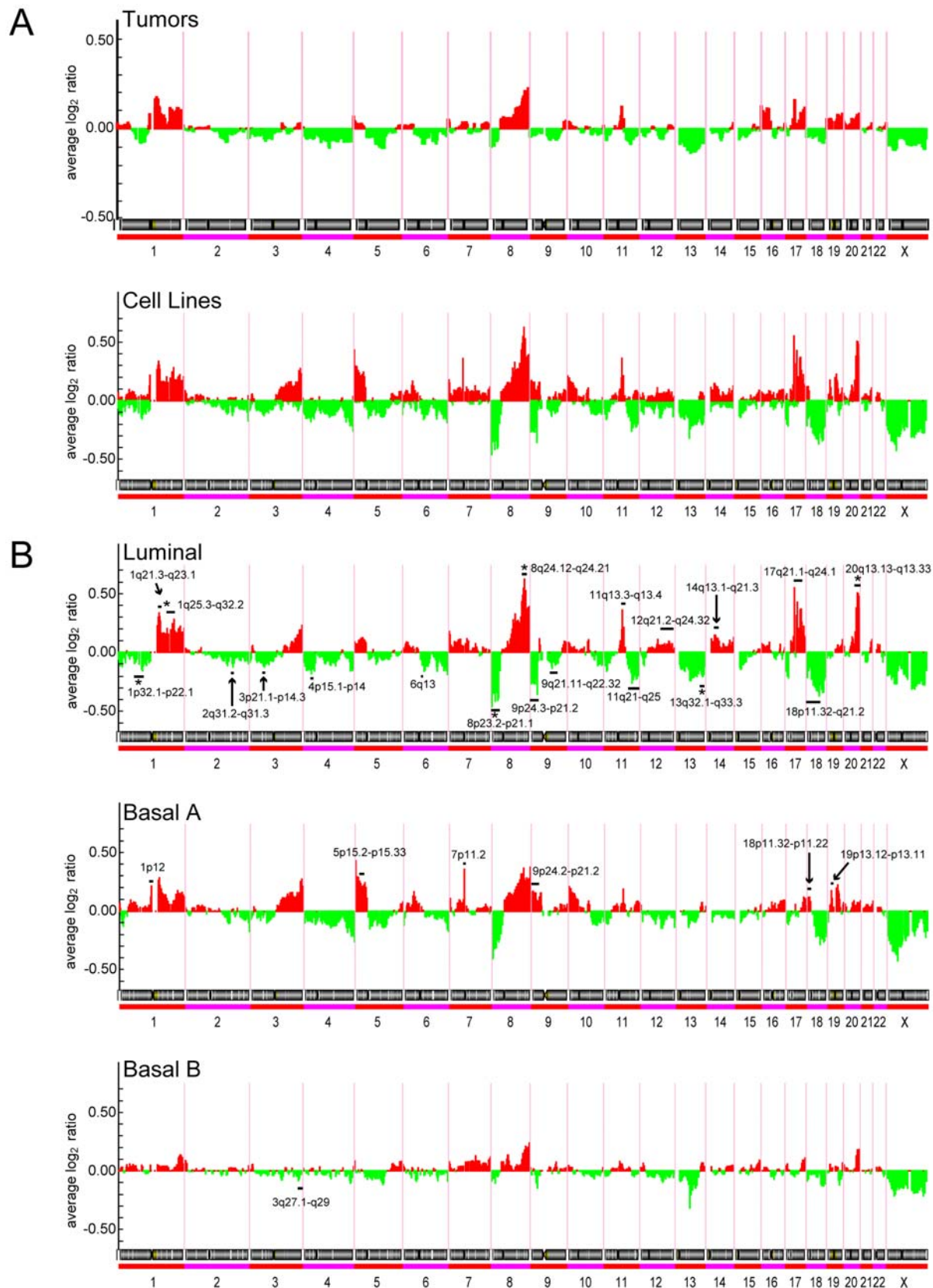


Figure 3. Genomic profiles define spectra of CNAs in cell line subtypes. (A) Spectra of gains (red) and losses (green), plotted as average \log_2 ratio, for 89 breast tumors [4], above, compared to the set of 50 cell lines (profiled for both expression and CNAs), below. (B) Spectra of gains and losses for the cell line subtypes: luminal (above), basal A (middle) and basal B (below). Statistically significant subtype-specific CNAs, called by SAM (FDR<5%), are marked by a black bar. The subset of those loci that also characterize the corresponding primary breast tumor subtype is marked by an asterisk.

doi:10.1371/journal.pone.0006146.g003

expression correlated significantly ($FDR < 0.05$) with altered gene copy number (Table S3). Of these, 487 resided within loci of high-amplitude CNA (Table 4). This subset included known breast cancer genes, like *EGFR* (7p11), *FGFR1* (8p12), *ERBB2* (17q12), *PPM1D* (17q23) and *ZNF217* (20q13). This subset is likely also enriched for novel breast cancer genes, and as such represents a rich source for cancer gene discovery. Notably, among the larger group of amplified/overexpressed genes are several with known functions relevant to oncogenesis, like cell proliferation (e.g. *EIF3H*, *HEY1*, *MELK*, *GAB2*, *CDC6*, *GRB2*) [42–47], survival (e.g. *HIPK1*, *MCL1*, *MAPKAPK2*, *VCP*, *VDAC2*, *APIP*, *MAP3K3*) [48–54], migration/invasion (e.g. *MUC1*, *ADAM9*, *SH3PXD2A*, *CD44*, *PAK1*, *GIT1*, *PTPN1*) [55–61], ER-signaling (e.g. *BCAS2*, *MUC1*, *NCOA3*, *TFAP2C*) [62–65], and maintenance of genome integrity (e.g. *NBN*, *RAD21*, *FANCG*, *BUB3*, *RAD9A*, *TAOK1*, *RAD51C*, *RAE1*) [66–73]. Also represented are several “druggable” classes [74], like kinases (e.g. *HIPK1*, *MAPKAPK2*, *MELK*, *RPS6KB2*, *PAK1*, *TAOK1*, *PIP4K2B*, *RPS6KB1*, *TLK2*, *MAP3K3*), phosphatases (e.g. *PTPN1*), proteases (e.g. *ADAM9*), G protein-coupled receptors (e.g. *GPRC5C*) and ion channels (e.g. *VDAC2*).

Discussion

Using whole-genome DNA microarrays, we collected transcriptional and genomic profiles across a set of 52 widely used breast cancer cell lines, with the primary goals to establish their suitability in modeling known breast tumor heterogeneity, and to create a resource for cancer gene discovery. Cluster analysis of transcriptional profiles defined three cell line subtypes, one luminal and two basal (A and B), consistent with other recent studies of breast cancer cell lines [31,33,75]. The luminal subtype included all ER-positive cell lines, and associated gene expression patterns reflected both ER and luminal differentiation pathways, the latter including *GATA3* and *FOXA1*, key transcriptional mediators of luminal differentiation [28,76]. The basal-like cell lines were ER-negative and exhibited more frequent mutations of *TP53* and *PTEN*, consistent with findings in basal-like tumors [3,77]. The basal-A subtype exhibited enriched expression of ETS pathway genes, a pathway linked to diverse tumor phenotypes including invasion and metastasis [78]. The basal-B subtype, which included the three non-tumorigenic lines (consistent with prior studies [75]), as well as five highly invasive/metastatic lines with features of EMT, exhibited enriched expression of EMT and EGF regulated genes, the latter pathway also previously linked to basal-like tumors [79].

Recently, Neve *et al.* [33] profiled 51 breast cancer cell lines (though using a lower-resolution (~1 Mb) CGH platform), 38 of which (~3/4th) overlapped with the 52 we profiled. All the overlapping lines except for one clustered into the same corresponding gene-expression subtype in both their and our study. The exception was HCC1500, which we classified as luminal while Neve *et al.* labeled it as basal B. The discrepancy may reflect a cell line identification error. We note that ATCC describes the line as ER-positive, more consistent with a luminal classification.

Our comparisons of expression profiles between breast cancer cell line subtypes and breast tumor subtypes provided valuable information relevant to the suitability of cell lines in modeling known breast tumor heterogeneity. Luminal-A/B tumors best matched luminal cell lines. Notably, basal-like tumors most corresponded to basal-A cell lines. Consistent with this finding, two breast cancer cell lines from *BRCA1* mutation carriers also clustered in basal-A (and basal-A lines exhibited enrichment of a *BRCA1* signature), where it has been established that *BRCA1*-associated tumors share many features with sporadic basal-like

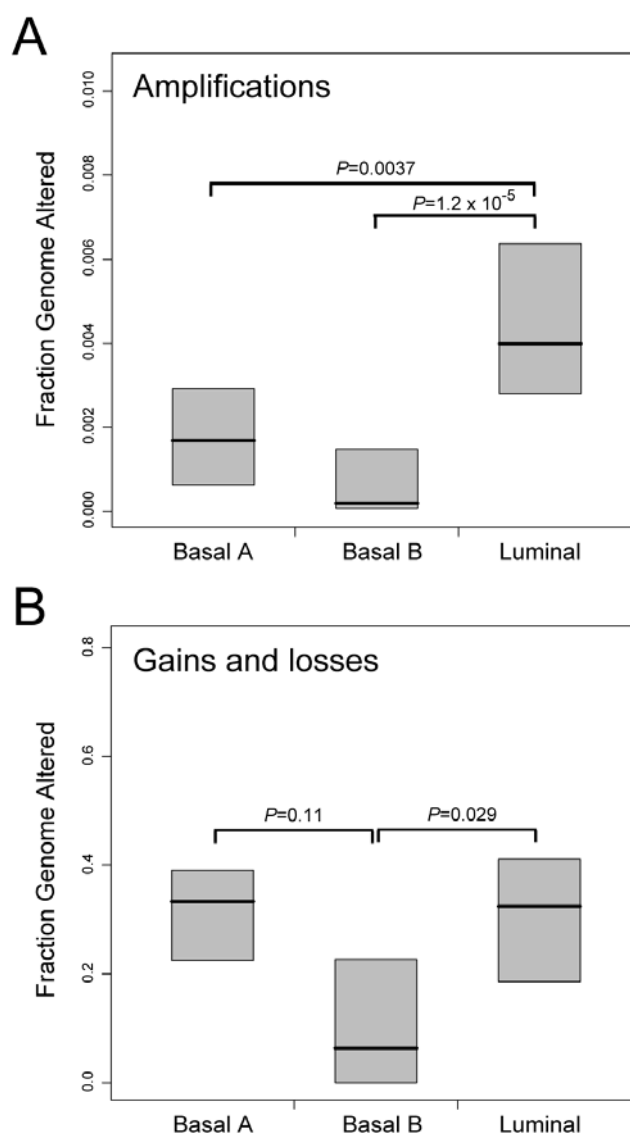


Figure 4. Cell line subtypes exhibit distinct genomic instabilities. Fraction of genome comprising (A) high-level DNA amplification; or (B) low-level gain/loss, stratified by cell line subtype (luminal, basal-A, basal-B). Box plots show 25th, 50th and 75th percentiles; *P*-values (Students *t*-test) for pairwise comparisons are shown. doi:10.1371/journal.pone.0006146.g004

tumors [80]. Interestingly, *ERBB2*-associated tumors matched both luminal and basal-A lines. While *ERBB2* represents a distinct expression tumor subtype in multiple independent cohorts [3,15,81], it is noteworthy that most *ERBB2* (*HER2*+) cell lines clustered in the luminal subtype. The basis for the discrepant *ERBB2* grouping in cell lines and tumors is unclear but warrants further investigation.

It has been suggested that the origin of the luminal *vs.* basal breast cancer distinction reflects the transformation of different breast epithelial progenitor cell compartments [82,83]. Breast epithelial stem/progenitor cells support mammary gland development during puberty and subsequent growth and remodeling during pregnancy [84]. A prevailing view is that breast epithelial stem cells give rise to bipotent basal/luminal progenitors, which then give rise to basal and luminal restricted progenitors, and from there to differentiated basal/myoepithelial and luminal epithelial

Table 4. High-amplitude amplifications and deletions.

Cytoband	P-Border (nt)	Q-Border (nt)	Size (kB)	Cell Lines [€]	Significant DNA-RNA Correlations [#]	Other notable genes [¶]
AMPLIFICATION						
1p32.2	56946690	57156366	210	EFM192A		
1p22.1-1p21.3	93549298	97052934	3504	SUM44*	DR1, FNBP1L, ARHGAP29, ALG14	
1p13.3	107738670	109306637	1568	HCC2688	C1orf59, PRPF38B, STXBP3, GPM2, CLCC1	VAV3
1p13.2	114220960	115183599	963	MCF7, UACC812	AP4B1, DCLRE1B, HIPK1, TRIM33, BCAS2, CSDE1, NRAS	
1q21.2	148738080	148885763	148	HCC1143	TAR52, MCL1 , ENSA, GOLPH3L	
1q21.2-q21.3	149460307	150130540	670	HCC712, UACC812	PIP5K1A, PSMD4, ZNF687, PI4KB, PSMB4, POGZ, SNX27, MRPL9	
1q21.3	151000411	151885402	885	HCC712		
1q22	153424958	153999982	575	UACC812	MUC1, C1orf2, CLK2, HCN3, PKLR, C1orf104, RUSC1, ASH1L, YY1AP1	
1q23.3	159283361	159357995	75	SUM190	KLHDC9	
1q32.1	204736293	205144756	408	UACC812	MAPKAPK2	IKBKE
3p14.2-p14.1	61765808	64574645	2809	MCF7		
3q26.32	178223920	180535525	2312	HCC2185	TBL1XR1, ZNF639	PIK3CA
3q29	194971434	195513283	542	HCC1937		
3q29	196883266	196931777	49	HCC1937		
4q12	53304442	54084198	780	HCC1007	SCFD2, FIP1L1	
5p15.33	712977	2811691	2099	HCC1954	ZDHHC11, PDCD6, MRPL36, NDUFS6	TERT
6p12.1	55358212	57236103	1878	HCC1007	KIAA11586, ZNF451, BAG2	
6q16.3-q21	104858272	109112665	4254	HCC2185	HACE1, ATG5, C6orf203, PDSS2, SEC63, OSTM1, SNX3, FOXO3A	
6q21-q22.31	111961945	123089199	11127	HCC2185	C6orf225, HDAC2, DSE, GOPC, NUS1, ASF1A, HSF2, SERINC1	
7p15.2	26557965	27107611	550	HCC1007		
7p11.2	54595526	55931398	1336	BT20, MDA468	EGFR	
7q21.13-q21.2	90779687	91868629	1089	SUM52	MTERF, AKAP9, CYP51A1, KRIT1, ANKIB1	
7q21.3	95239813	96489919	1250	SUM52	SLC25A13, SHFM1	
7q22.1	100294293	100421513	127	SUM52	SLC12A9	
8p21.3	21593811	21966432	373	MDA134	XPO7	
8p12-p11.21	32328805	41907423	9579	BT483, HCC1500, HCC1599, MDA134, SUM44*, SUM52	FUT10, C8orf41, MAK16, ZNF703, ERLIN2, PROSC, BRF2, RAB11FIP1, EIF4EBP1, ASH2L, LSM1, BAG4, DDHD2, WHSC1L1, LETM2, FGFR1 , TACC1, PLEKHA2, TM2D2, ADAM9, GOLGA7, AGPAT6	IKBKB
8q12.2-q12.3	61817956	62960675	1143	SUM190	CHD7	
8q13.3	71707355	72999610	1292	SKBR3		
8q21.11-q21.13	79781799	85260376	5479	EFM192A, HCC1419, HCC1599, SKBR3	HEY1, TPD52, ZBTB10	
8q21.3-q22.1	89113344	95233478	6120	EFM192A, HCC1419, SKBR3	OSGIN2, NBN, DECR1, OTUD6B, RBM12B, TMEM67	
8q22.2-q22.3	100879473	101995283	1116	HCC1419, HCC2185	COX6C, POLR2K	
8q22.3	104311423	104550566	239	HCC1419	FZD6	
8q23.1-q24.21	108267427	131134620	22867	EFM192A, HCC1419, HCC1599, HCC2185, SKBR3, ZR75-30	EIF3E, TRPS1, EIF3H, C8orf53, RAD21, TAF2, DSCC1, MRPL13, MTBP, DERL1, WDR67, C8orf76, ZHX1, ATAD2, C8orf32, FAM91A1, TMEM65, TRMT12, RNF139, TATDN1, NDUFB9, SQLE, KIAA0196, NSMCE2, FAM84B	MYC
8q24.22	133917771	134337653	420	ZR75-30	PHF20L1	
8q24.3	141658961	143348731	1690	HCC1419, MDA436, ZR75-30	GPR20, FLJ43860	
8q24.3	144310706	144753628	443	MDA436, ZR75-30	ZFP41, GLI4, ZNF696, C8orf51, RHPN1, MAFA	

Table 4. Cont.

Cytoband	P-Border (nt)	Q-Border (nt)	Size (kB)	Cell Lines ^e	Significant DNA-RNA Correlations [#]	Other notable genes ^a
8q24.3	145137850	146252219	1114	BT483, HCC1419, MDA436, ZR75-30	GRINA, OPLAH, SHARPIN, KIAA1833, FBXL6, CPSF1, VPS28, KIFC2, ZNF252	
9p13.3-p13.2	33876876	38058023	4181	HCC2185	UBE2R2, UBAP2, WDR40A, KIF24, KIAA1161, DCTN3, GALT, IL11RA, VCP, FANCG, PIGO, STOML2, RUSC2, TESK1, CD72, C9orf100, TLN1, CREB3, RGP1, HINT2, CLTA, RNF38, MELK, ZCCHC7, GRHPR, ZBTB5, POLR1E, FBXO10, RG9MTD3, WDR32, MCART1	
9q33.3	128307884	129195638	888	SUM44*	RALGPS1	
10q21.1-q21.2	72507196	73797267	1290	HCC2157	DNAJB12	
10q22.2-q22.3	76461776	82106491	5645	EFM19, HCC2157	SAMD8, VDAC2, DLG5, POLR3A, RPS24, LOC283050, ZMIZ1, PPIF, SFTPA1, FAM22E, C10orf57, ANXA11	
10q24.33-q25.1	105307581	106054698	747	EFM19	SH3PXD2A	
10q26.13	124598599	124962466	364	SUM52	IKZF5, BUB3	
11p13	33062705	35600197	2537	HCC1806*	HIPK3, FBXO3, CAPRIN1, NAT10, ABTB2, CAT, APIP, PDHX, CD44	
11q13.2	66874536	67198753	324	MDA134, ZR75-1	RAD9A, RPS6KB2, CORO1B, TMEM134	
11q13.3-q13.4	68427956	70812048	2384	HCC1143, HCC1500, HCC1954, MDA134, MDA175, MDA361, SUM44*, SUM190,	IGHMBP2, FADD, PPFIA1, CTTN, SHANK2	CCND1
11q13.4	73316198	73649077	333	BT474, MDA134, SUM190	UCP2, C2CD3, PPME1	
11q13.4-q14.1	74648813	77963474	3315	MDA134, SUM44*, SUM52, SUM190	ARRB1, PRKRIR, EMSY , PHCA, PAK1, AQP11, CLNS1A, C11orf67, INTS4, NDUFC2, ALG8, GAB2, NARS2	
12p12.3	18727378	19246201	519	HCC1500		
12q21.31-q21.33	88265969	88443930	178	SUM52	WDR51B, GALNT4	
13q22.2-q31.1	74756931	78096263	3339	UACC812	UCHL3	
13q31.3-q32.1	90798074	93942902	3145	UACC812		
16q12.2	51800892	53524601	1724	EFM19, SUM44*	CHD9, FTO	
17p12	12611513	13636592	1025	EFM192A	ELAC2	
17q11.2	23686912	24013273	326	ZR75-30	POLDIP2, TREM199, SLC46A1, PIGS, SPAG5, FLJ25006, KIAA0100, SDF2	
17q11.2	24894649	25818484	924	HCC202	TAOK1, LOC116236, GIT1, ANKRD13B, CPD	
17q11.2	27727543	28293356	566	SUM190	ZNF207	
17q12	31206068	31649844	444	MDA361	FLJ12120	
17q12-q21.2	32627885	36209712	3582	BT474, EFM192A, HCC202, HCC1419, HCC1569, HCC1954, HCC2218, MDA361, SKBR3, SUM190, UACC812, UACC893, ZR75-30	ACACA, TADA2L, DDX52, SOCS7, MLLT6, C1SD3, PCGF2, PSMB3, PIP4K2B, CCDC49, RPL23, LASP1, CACNB1, FAM153C, RPL19, LOC90110, FBXL20, MED1, PPP1R1B, STARD3, TCAP, PERLD1, ERBB2 , C17orf37, GRB7, IKZF3, GSDML, ORMDL3, PSMD3, MED24, MSL-1, CASC3, CDC6, RARA, SMARCE1	
17q21.31	38419019	38738864	320	SUM190	RND2	
17q21.32-q25.1	43329972	50826668	7497	BT474, EFM192A, HCC202, HCC712, HCC1419, HCC2218, ZR75-30	SP2, PNPO, CDK5RAP3, SNX11, HOXB13, CALCOCO2, ATP5G1, UBE2Z, SNF8, ZNF652, PHB, SPOP, SLC35B1, FAM117A, MYST2, PDK2, XYLT2, MRPL27, LRRC59, EME1, ACSF2, RSAD1, EPN3, SPATA20, ABCC3, ANKRD40, CROP, TOB1, NME1, TOM1L1, COX11, STXBPA	
17q23.2-q24.2	53282667	63106134	9823	BT474, HCC712, HCC2218, MCF7, MDA361, ZR75-30	SFRS1, DYNLL2, MKS1, SUPT4H1, MTMR4, RAD51C, TRIM37, FAM33A, C17orf71, YPEL2, DHX40, CLTC, PTRH2, TMEM49, TUBD1, RPS6KB1 , RNFT1, HEATR6, USP32, APPBP2, PPM1D , BRIP1, INTS2, MED13, METTL2A, TLK2, TANC2, CYB561, WDR68, CCDC44, MAP3K3, LYK5, CCDC47, DDX42, PSMD5, SMARCD2, DDX5, CCDC45, SMURF2, GNA13, HELZ	

Table 4. Cont.

Cytoband	P-Border (nt)	Q-Border (nt)	Size (kB)	Cell Lines [€]	Significant DNA-RNA Correlations [#]	Other notable genes ^{**}
17q25.1	69755691	71418122	1662	HCC2218, MDA361, MDA453, UACC893	GPRC5C, SLC9A3R1, NAT9, TMEM104, FDXR, C17orf28, CDR2L, ICT1, KCTD2, SUMO2, NUP85, GGA3, MRP57, MIF4GD, SLC25A19, GRB2, CASKIN2, TSEN54, MYO15B, SAP30BP, H3F3B, UNK, WBP2	
18q21.32-q21.33	55178911	57628085	2449	HCC1500		
19p13.2	14932742	15602448	670	HCC1143	ILVBL, BRD4, AKAP8L	
19q12-q13.11	33966349	38052482	4086	HCC1569, HCC1599	UQCRF51, POP4, PLEKHF1, C19orf2, DPY19L3, ANKRD27	
19q13.11	39866832	40146793	280	HCC1599		
19q13.42	60551045	60898029	347	EFM19	FIZ1, ZNF784, CCDC106	
19q13.43	63208125	63774724	567	HCC1806*	ZNF329, ZNF274, ZNF8, ZSCAN22, ZNF324, TRIM28, CHMP2A, UBE2M	
20p12.2	10224083	10433564	209	HCC2185	MKKS	
20q11.22	32363269	33563203	1200	BT474	DYNLRB1, NCOA6, UQCC	
20q13.12	42493067	43286511	793	BT474, SUM52	SERINC3	
20q13.12-q13.13	45234836	48636574	3402	BT474, HCC1419, MCF7	NCOA3, PREX1, ARFGEF2, STAU1, DDX27, ZNFX1, SLC9A8, SPATA2, PTPN1	
20q13.13-q13.32	49139330	57334442	8195	BT474, HCC1419, MCF7, SKBR3	ZFP64, ZNF217 , BCAS1, PFDN4, C20orf108, CSTF1, C20orf43, TFAP2C, BMP7, RAE1, RBM38, RAB22A, VAPB, STX16, NPEPL1, GNAS, TH1L, ATP5E, SLMO2	AURKA
20q13.33	61801252	62370522	569	HCC1419	PRR17, OPRL1	
22q11.21	18256420	19686015	1430	SUM190	COMT, HTF9C, PI4KA	
22q12.1	24895479	25885840	990	HCC202	HPS4	
Xp11.23-p11.22	48635684	51225253	2590	HCC712		
Xp11.22	52255712	54236019	1980	HCC202	TMEM29, PHF8	
Xq28	148368959	149592006	1223	HCC202		
DELETION						
6q16.3-q21	102493055	105832848	3340	HCC1395	HACE1	
7q11.23-q21.11	77246720	77484743	238	HCC1806*	TMEM60, PHTF2	
8p23.3	604200	2080787	1477	HCC2688	ERICH1	
9p24.3-p24.2	958704	3213008	2254	HCC2185	VLDLR, KIAA0020	
9p21.2-p21.1	26894518	29207861	2313	BT474, EFM19	PLAA, IFT74	CDKN2A
13q14.3-13q21.2	52175620	60001053	7825	HCC1395		
15q24.3	74984799	75116728	132	HCC1806*	RCN2	
17p12	11405197	11987872	583	EFM19	MAP2K4	
17q21.31	38252285	38419019	167	HCC1806*		BRCA1
18q11.2-q12.1	22256956	23913060	1656	HCC2185		
21q21.1	18342236	21590772	3249	ZR75-30		
Xp11.3	46208136	46345060	137	HCC2157		
Xq25	122657657	123338533	681	HCC1806*		

[€]For aberrations spanning multiple lines, inclusive interval indicated.

^{*}DNA but not RNA profiled.

[#]Only named genes listed, ordered by genome position; bold text indicates select known cancer genes.

^{**}Within or immediately flanking interval.

doi:10.1371/journal.pone.0006146.t004

cells [84,85]. Bipotent human breast epithelial stem/progenitors have been characterized with the cell surface phenotype $MUC^{-/low}/CALLA^{low/+}$ [39]. Separately, breast cancer stem cells, identified prospectively as tumor initiating cells when transplanted into immunodeficient mice, have been characterized by the surface expression phenotype $CD44^{+}/CD24^{-/low}$ [40], also

a presumed phenotype of normal breast epithelial stem or early progenitor cells [84].

Our transcriptional profiles of breast cancer cell lines are consistent with an origin in (or at least a likeness of the bulk cell population to) the various stem/progenitor cell compartments. Basal-B lines predominantly express $CD44^{+}/CD24^{-/low}$ and

MUC⁻/CALLA⁺ phenotypes characteristic of stem or bipotent progenitor cells, as well as ITGB3 (CD61), also recently characterized as a cancer stem cell marker in MMTV-wnt-1 induced murine breast cancer [41]. In contrast, basal-A lines appear mainly CD44⁺/CD24⁺, but express PROM1 (aka CD133), a marker of luminal progenitors in mice [86] also more recently characterized as a stem cell marker in BRCA1-associated breast cancer [87], while luminal lines express markers of luminal lineage restriction like GATA3 and FOXA1 [28]. Conspicuously absent from our analysis is a breast tumor subtype corresponding to the stem-cell like (and sometimes mesenchymal-like) basal-B lines. Whether basal-B lines reflect an uncommon tumor subtype not yet characterized, or else a stem/progenitor subpopulation of tumor cells enriched in culture, or even an artifact of cell culture, remains to be determined. Regardless, breast cancer cell lines are likely to prove useful for discovering new stem cell markers, and for studying stem/progenitor cell biology.

Our genomic profiles of breast cancer cell lines indicate that overall the spectra of CNAs is reflective of breast tumors, consistent with prior findings from loss of heterozygosity (LOH) analysis [11]. Overall, however, cell lines exhibited higher frequencies and greater complexities of CNAs, and seemingly more than might be explained by a higher sensitivity of detecting CNAs in stromal-free tumor cell populations. Notably absent among the luminal subtype were the “simple” karyotypes characteristic of luminal-A tumors (i.e. 1q+, 16p+/16q-). By genomic profiles, luminal cell lines shared features characteristic of luminal-B tumors, including certain subtype-specific CNAs and overall higher levels of DNA amplification. Likewise, basal-A cell lines and basal-like tumors shared the feature of high levels of chromosome segment gain/loss. However, overall only a subset of subtype-specific CNAs was preserved. Therefore, at the genomic level it is uncertain how well cell line subtypes faithfully represent tumor subtype counterparts.

Taken together, the transcriptional and genomic profiles support the conclusion that luminal and basal-A cell lines are the most appropriate cell line models of luminal-B and basal-like tumors, respectively. Further, the basal lines are likely useful models for biological studies of the 70-gene, wound and hypoxia signatures. Despite incongruent expression results, luminal lines with amplification/overexpression of ERBB2 are likely appropriate models of ERBB2-associated tumors. Our findings indicate that new cell lines are needed to more faithfully model luminal-A tumors. Currently available cell lines likely reflect certain biases in the specimen source of cell line, and/or in the culturing methods, as suggested by the predominance of HCC lines (from UT Southwestern) among the basal-A group. Different culturing methods (e.g. ref. [88]) might support the establishment of cell lines from luminal-A tumors.

Our genomic profiles also identified numerous high-level DNA amplifications and multi-copy deletions, pinpointing known and novel cancer genes. Further, by integrating the genomic and transcriptional datasets, we could define a set of candidate cancer

genes residing at these loci and exhibiting both altered copy number and expression. The larger set of amplified/overexpressed genes included several known breast cancer oncogenes, as well as many plausible candidates including genes with known functions relevant to carcinogenesis, like cell proliferation, survival and motility/invasion, and genome integrity (e.g. DNA damage response). Though genes maintaining genome integrity are more typically considered candidate tumor suppressors, the overexpression of such genes has been linked to genome instability [67,89]. The set of amplified/overexpressed genes also included many druggable targets [74], most notably several kinases. Importantly, the same cell lines used for discovery can also be used to functionally examine cancer gene candidates, for example using RNA interference to knockdown the expression of amplified oncogene candidates, and then assaying loss of tumorigenic phenotypes in cultured cells or *in vivo* (e.g. refs.[90,91]). Indeed, high-throughput RNA interference approaches [92,93] might be used to evaluate many or all of the candidate cancer genes simultaneously.

In summary, transcriptional and genomic profiling of 52 commonly used breast cancer cell lines identifies cell line subtypes, and defines the cell line subtypes that most faithfully capture the known heterogeneity of breast tumors. Specifically, luminal and basal-A lines appear to best model the features of luminal-B and basal-like tumors, while basal-B lines might inform stem cell biology. In addition, our integrated analysis of genomic and transcriptional profiles pinpoints loci and genes with altered copy number and expression, providing a rich source for discovery and future characterization of new breast cancer genes.

Supporting Information

Table S1 8,750 variably expressed genes (log2 ratios)

Found at: doi:10.1371/journal.pone.0006146.s001 (1.11 MB ZIP)

Table S2 Processed aCGH data (log2 ratios)

Found at: doi:10.1371/journal.pone.0006146.s002 (2.82 MB ZIP)

Table S3 Genes with significantly correlated copy number and expression

Found at: doi:10.1371/journal.pone.0006146.s003 (0.13 MB TXT)

Acknowledgments

We wish to thank the SFGF for microarray manufacture, SMD for database support, and members of the Pollack lab for helpful discussion.

Author Contributions

Conceived and designed the experiments: JK KS LG JKG AFG JDM JRP. Performed the experiments: JK KS MB YLC LG JKG KAK. Analyzed the data: JK KS MB JKG THB PW AFG JDM JRP. Contributed reagents/materials/analysis tools: KS LG THB AFG JDM. Wrote the paper: JK KS JRP.

References

1. Subramaniam DS, Isaacs C (2005) Utilizing prognostic and predictive factors in breast cancer. *Curr Treat Options Oncol* 6: 147–159.
2. Perou CM, Sorlie T, Eisen MB, van de Rijn M, Jeffrey SS, et al. (2000) Molecular portraits of human breast tumours. *Nature* 406: 747–752.
3. Sorlie T, Perou CM, Tibshirani R, Aas T, Geisler S, et al. (2001) Gene expression patterns of breast carcinomas distinguish tumor subclasses with clinical implications. *Proc Natl Acad Sci U S A* 98: 10869–10874.
4. Bergamaschi A, Kim YH, Wang P, Sorlie T, Hernandez-Boussard T, et al. (2006) Distinct patterns of DNA copy number alteration are associated with different clinicopathological features and gene-expression subtypes of breast cancer. *Genes Chromosomes Cancer* 45: 1033–1040.
5. Chin K, DeVries S, Fridlyand J, Spellman PT, Roydasgupta R, et al. (2006) Genomic and transcriptional aberrations linked to breast cancer pathophysiology. *Cancer Cell* 10: 529–541.
6. Lacroix M, Leclercq G (2004) Relevance of breast cancer cell lines as models for breast tumours: an update. *Breast Cancer Res Treat* 83: 249–289.
7. Vargo-Gogola T, Rosen JM (2007) Modelling breast cancer: one size does not fit all. *Nat Rev Cancer* 7: 659–672.

8. Livak KJ, Schmittgen TD (2001) Analysis of relative gene expression data using real-time quantitative PCR and the 2-(Delta Delta C(T)) Method. *Methods* 25: 402–408.
9. Potemski P, Pluciennik E, Bednarek AK, Kusinska R, Kubiak R, et al. (2007) Evaluation of oestrogen receptor expression in breast cancer by quantification of mRNA. *Histopathology* 51: 829–836.
10. Sato M, Vaughan MB, Girard L, Peyton M, Lee W, et al. (2006) Multiple oncogenic changes (K-RAS(V12), p53 knockdown, mutant EGFRs, p16 bypass, telomerase) are not sufficient to confer a full malignant phenotype on human bronchial epithelial cells. *Cancer Res* 66: 2116–2128.
11. Wistuba II, Behrens C, Milchgrub S, Syed S, Ahmadian M, et al. (1998) Comparison of features of human breast cancer cell lines and their corresponding tumors. *Clin Cancer Res* 4: 2931–2938.
12. Bergamaschi A, Kim YH, Kwei KA, Choi Y-L, Bocanegra M, et al. (2008) CAMK1D amplification implicated in epithelial-mesenchymal transition in basal-like breast cancer. *Molecular Oncology* 2: 327–339.
13. Demeter J, Beauheim C, Gollub J, Hernandez-Boussard T, Jin H, et al. (2007) The Stanford Microarray Database: implementation of new analysis tools and open source release of software. *Nucleic Acids Res* 35: D766–770.
14. Subramanian A, Tamayo P, Mootha VK, Mukherjee S, Ebert BL, et al. (2005) Gene set enrichment analysis: a knowledge-based approach for interpreting genome-wide expression profiles. *Proc Natl Acad Sci U S A* 102: 15545–15550.
15. Sorlie T, Tibshirani R, Parker J, Hastie T, Marron JS, et al. (2003) Repeated observation of breast tumor subtypes in independent gene expression data sets. *Proc Natl Acad Sci U S A* 100: 8418–8423.
16. Tusher VG, Tibshirani R, Chu G (2001) Significance analysis of microarrays applied to the ionizing radiation response. *Proc Natl Acad Sci U S A* 98: 5116–5121.
17. van't Veer LJ, Dai H, van de Vijver MJ, He YD, Hart AA, et al. (2002) Gene expression profiling predicts clinical outcome of breast cancer. *Nature* 415: 530–536.
18. Chang HY, Sneddon JB, Alizadeh AA, Sood R, West RB, et al. (2004) Gene Expression Signature of Fibroblast Serum Response Predicts Human Cancer Progression: Similarities between Tumors and Wounds. *PLoS Biol* 2: E7.
19. Chi JT, Wang Z, Nuyten DS, Rodriguez EH, Schaner ME, et al. (2006) Gene expression programs in response to hypoxia: cell type specificity and prognostic significance in human cancers. *PLoS Med* 3: e47.
20. Schuler GD (1997) Pieces of the puzzle: expressed sequence tags and the catalog of human genes. *J Mol Med* 75: 694–698.
21. Pollack JR, Perou CM, Alizadeh AA, Eisen MB, Pergamenschikov A, et al. (1999) Genome-wide analysis of DNA copy-number changes using cDNA microarrays. *Nat Genet* 23: 41–46.
22. Pollack JR, Sorlie T, Perou CM, Rees CA, Jeffrey SS, et al. (2002) Microarray analysis reveals a major direct role of DNA copy number alteration in the transcriptional program of human breast tumors. *Proc Natl Acad Sci U S A* 99: 12963–12968.
23. Tibshirani R, Wang P (2008) Spatial smoothing and hot spot detection for CGH data using the fused lasso. *Biostatistics* 9: 18–29.
24. Gudas JM, Klein RC, Oka M, Cowan KH (1995) Posttranscriptional regulation of the c-myc proto-oncogene in estrogen receptor-positive breast cancer cells. *Clin Cancer Res* 1: 235–243.
25. Boulay A, Breuleux M, Stephan C, Fux C, Brisken C, et al. (2008) The Ret receptor tyrosine kinase pathway functionally interacts with the ERalpha pathway in breast cancer. *Cancer Res* 68: 3743–3751.
26. Inoue A, Omoto Y, Yamaguchi Y, Kiyama R, Hayashi SI (2004) Transcription factor EGR3 is involved in the estrogen-signaling pathway in breast cancer cells. *J Mol Endocrinol* 32: 649–661.
27. Jeltsch JM, Roberts M, Schatz C, Garnier JM, Brown AM, et al. (1987) Structure of the human oestrogen-responsive gene pS2. *Nucleic Acids Res* 15: 1401–1414.
28. Kouros-Mehr H, Slorach EM, Sternlicht MD, Werb Z (2006) GATA-3 maintains the differentiation of the luminal cell fate in the mammary gland. *Cell* 127: 1041–1055.
29. Jones C, Mackay A, Grigoriadis A, Cossu A, Reis-Filho JS, et al. (2004) Expression profiling of purified normal human luminal and myoepithelial breast cells: identification of novel prognostic markers for breast cancer. *Cancer Res* 64: 3037–3045.
30. Nielsen TO, Hsu FD, Jensen K, Cheang M, Karaca G, et al. (2004) Immunohistochemical and clinical characterization of the basal-like subtype of invasive breast carcinoma. *Clin Cancer Res* 10: 5367–5374.
31. Charafe-Jauffret E, Ginestier C, Monville F, Finetti P, Adelaide J, et al. (2006) Gene expression profiling of breast cell lines identifies potential new basal markers. *Oncogene* 25: 2273–2284.
32. Charafe-Jauffret E, Monville F, Bertucci F, Esterni B, Ginestier C, et al. (2007) Moesin expression is a marker of basal breast carcinomas. *Int J Cancer* 121: 1779–1785.
33. Neve RM, Chin K, Fridlyand J, Yeh J, Bachner FL, et al. (2006) A collection of breast cancer cell lines for the study of functionally distinct cancer subtypes. *Cancer Cell* 10: 515–527.
34. Tomlinson GE, Chen TT, Stastny VA, Virmani AK, Spillman MA, et al. (1998) Characterization of a breast cancer cell line derived from a germ-line BRCA1 mutation carrier. *Cancer Res* 58: 3237–3242.
35. Neuzil J, Stantic M, Zabalova R, Chladova J, Wang X, et al. (2007) Tumour-initiating cells vs. cancer 'stem' cells and CD133: what's in the name? *Biochem Biophys Res Commun* 355: 855–859.
36. Bae SN, Arand G, Azzam H, Pavasant P, Torri J, et al. (1993) Molecular and cellular analysis of basement membrane invasion by human breast cancer cells in Matrigel-based in vitro assays. *Breast Cancer Res Treat* 24: 241–255.
37. Holst-Hansen C, Johannessen B, Hoyer-Hansen G, Romer J, Ellis V, et al. (1996) Urokinase-type plasminogen activation in three human breast cancer cell lines correlates with their in vitro invasiveness. *Clin Exp Metastasis* 14: 297–307.
38. Dumont N, Bakin AV, Arteaga CL (2003) Autocrine transforming growth factor-beta signaling mediates Smad-independent motility in human cancer cells. *J Biol Chem* 278: 3275–3285.
39. Stingl J, Eaves CJ, Zandieh I, Emerman JT (2001) Characterization of bipotent mammary epithelial progenitor cells in normal adult human breast tissue. *Breast Cancer Res Treat* 67: 93–109.
40. Al-Hajj M, Wicha MS, Benito-Hernandez A, Morrison SJ, Clarke MF (2003) Prospective identification of tumorigenic breast cancer cells. *Proc Natl Acad Sci U S A* 100: 3983–3988.
41. Vaillant F, Asselin-Labat ML, Shackleton M, Forrest NC, Lindeman GJ, et al. (2008) The mammary progenitor marker CD61/beta3 integrin identifies cancer stem cells in mouse models of mammary tumorigenesis. *Cancer Res* 68: 7711–7717.
42. Zhang L, Smit-McBride Z, Pan X, Rheinhardt J, Hershey JW (2008) An oncogenic role for the phosphorylated h-subunit of human translation initiation factor eIF3. *J Biol Chem*.
43. Hulleman E, Quarto M, Vernell R, Masserdotti G, Colli E, et al. (2008) A role for the transcription factor HEY1 in glioblastoma. *J Cell Mol Med*.
44. Gray D, Jubb AM, Hogue D, Dowd P, Kijavini N, et al. (2005) Maternal embryonic leucine zipper kinase/murine protein serine-threonine kinase 38 is a promising therapeutic target for multiple cancers. *Cancer Res* 65: 9751–9761.
45. Tari AM, Hung MC, Li K, Lopez-Berestein G (1999) Growth inhibition of breast cancer cells by Grb2 downregulation is correlated with inactivation of mitogen-activated protein kinase in EGFR, but not in ErbB2, cells. *Oncogene* 18: 1325–1332.
46. Borlado LR, Mendez J (2008) CDC6: from DNA replication to cell cycle checkpoints and oncogenesis. *Carcinogenesis* 29: 237–243.
47. Bentes-Alj M, Gil SG, Chan R, Wang ZC, Wang Y, et al. (2006) A role for the scaffolding adapter GAB2 in breast cancer. *Nat Med* 12: 114–121.
48. Kondo S, Lu Y, Debbas M, Lin AW, Sarosi I, et al. (2003) Characterization of cells and gene-targeted mice deficient for the p53-binding kinase homeodomain-interacting protein kinase 1 (HIPK1). *Proc Natl Acad Sci U S A* 100: 5431–5436.
49. Reynolds JE, Yang T, Qian L, Jenkinson JD, Zhou P, et al. (1994) Mcl-1, a member of the Bcl-2 family, delays apoptosis induced by c-Myc overexpression in Chinese hamster ovary cells. *Cancer Res* 54: 6348–6352.
50. Reinhardt HC, Aslanian AS, Lees JA, Yaffe MB (2007) p53-deficient cells rely on ATM- and ATR-mediated checkpoint signaling through the p38MAPK/MK2 pathway for survival after DNA damage. *Cancer Cell* 11: 175–189.
51. Vandermoere F, El Yazidi-Belkoura I, Slomianky C, Demont Y, Bidaux G, et al. (2006) The valosin-containing protein (VCP) is a target of Akt signaling required for cell survival. *J Biol Chem* 281: 14307–14313.
52. Cheng EH, Sheiko TV, Fisher JK, Craigen WJ, Korsmeyer SJ (2003) VDAC2 inhibits BAK activation and mitochondrial apoptosis. *Science* 301: 513–517.
53. Cho DH, Lee HJ, Kim HJ, Hong SH, Pyo JO, et al. (2007) Suppression of hypoxic cell death by AP1-induced sustained activation of AKT and ERK1/2. *Oncogene* 26: 2809–2814.
54. Samanta AK, Huang HJ, Bast RC Jr, Liao WS (2004) Overexpression of MEKK3 confers resistance to apoptosis through activation of Nf-kappaB. *J Biol Chem* 279: 7576–7583.
55. Schroeder JA, Adriance MC, Thompson MC, Camenisch TD, Gendler SJ (2003) MUC1 alters beta-catenin-dependent tumor formation and promotes cellular invasion. *Oncogene* 22: 1324–1332.
56. Mazzocca A, Coppari R, De Franco R, Cho JY, Libermann TA, et al. (2005) A secreted form of ADAM9 promotes carcinoma invasion through tumor-stromal interactions. *Cancer Res* 65: 4728–4738.
57. Seals DF, Azucena EF Jr, Pass I, Tesfay L, Gordon R, et al. (2005) The adaptor protein Tks5/Fish is required for podosome formation and function, and for the protease-driven invasion of cancer cells. *Cancer Cell* 7: 155–165.
58. Marhaba R, Zoller M (2004) CD44 in cancer progression: adhesion, migration and growth regulation. *J Mol Histol* 35: 211–231.
59. Adam L, Vadlamudi R, Mandal M, Chernoff J, Kumar R (2000) Regulation of microfilament reorganization and invasiveness of breast cancer cells by kinase dead p21-activated kinase-1. *J Biol Chem* 275: 12041–12050.
60. Manabe R, Kovalenko M, Webb DJ, Horwitz AR (2002) GIT1 functions in a motile, multi-molecular signaling complex that regulates protrusive activity and cell migration. *J Cell Sci* 115: 1497–1510.
61. Cheng A, Bal GS, Kennedy BP, Tremblay ML (2001) Attenuation of adhesion-dependent signaling and cell spreading in transformed fibroblasts lacking protein tyrosine phosphatase-1B. *J Biol Chem* 276: 25848–25855.
62. Qi C, Zhu YT, Chang J, Yeldandi AV, Rao MS, et al. (2005) Potentiation of estrogen receptor transcriptional activity by breast cancer amplified sequence 2. *Biochem Biophys Res Commun* 328: 393–398.

63. Wei X, Xu H, Kufe D (2006) MUC1 oncoprotein stabilizes and activates estrogen receptor alpha. *Mol Cell* 21: 295–305.
64. Anzick SL, Kononen J, Walker RL, Azorsa DO, Tanner MM, et al. (1997) AIB1, a steroid receptor coactivator amplified in breast and ovarian cancer. *Science* 277: 965–968.
65. Woodfield GW, Horan AD, Chen Y, Weigel RJ (2007) TFAP2C controls hormone response in breast cancer cells through multiple pathways of estrogen signaling. *Cancer Res* 67: 8439–8443.
66. Varon R, Vissinga C, Platzter M, Cerosaletti KM, Chrzanowska KH, et al. (1998) Nibrin, a novel DNA double-strand break repair protein, is mutated in Nijmegen breakage syndrome. *Cell* 93: 467–476.
67. Hauf S, Waizenegger IC, Peters JM (2001) Cohesin cleavage by separase required for anaphase and cytokinesis in human cells. *Science* 293: 1320–1323.
68. Kawabe T, Tsuyama N, Kitao S, Nishikawa K, Shimamoto A, et al. (2000) Differential regulation of human RecQ family helicases in cell transformation and cell cycle. *Oncogene* 19: 4764–4772.
69. Yamamoto K, Ishiai M, Matsushita N, Arakawa H, Lamerdin JE, et al. (2003) Fanconi anemia FANCG protein in mitigating radiation- and enzyme-induced DNA double-strand breaks by homologous recombination in vertebrate cells. *Mol Cell Biol* 23: 5421–5430.
70. Babu JR, Jeganathan KB, Baker DJ, Wu X, Kang-Decker N, et al. (2003) Rael is an essential mitotic checkpoint regulator that cooperates with Bub3 to prevent chromosome missegregation. *J Cell Biol* 160: 341–353.
71. Volkmer E, Karnitz LM (1999) Human homologs of *Schizosaccharomyces pombe* rad1, hus1, and rad9 form a DNA damage-responsive protein complex. *J Biol Chem* 274: 567–570.
72. Draviam VM, Stegmeier F, Nalepa G, Sowa ME, Chen J, et al. (2007) A functional genomic screen identifies a role for TAO1 kinase in spindle-checkpoint signalling. *Nat Cell Biol* 9: 556–564.
73. French CA, Masson JY, Griffin CS, O'Regan P, West SC, et al. (2002) Role of mammalian RAD51L2 (RAD51C) in recombination and genetic stability. *J Biol Chem* 277: 19322–19330.
74. Hopkins AL, Groom CR (2002) The druggable genome. *Nat Rev Drug Discov* 1: 727–730.
75. Ross DT, Perou CM (2001) A comparison of gene expression signatures from breast tumors and breast tissue derived cell lines. *Dis Markers* 17: 99–109.
76. Asselin-Labat ML, Sutherland KD, Barker H, Thomas R, Shackleton M, et al. (2007) Gata-3 is an essential regulator of mammary-gland morphogenesis and luminal-cell differentiation. *Nat Cell Biol* 9: 201–209.
77. Saal LH, Gruvberger-Saal SK, Persson C, Lovgren K, Juppmanen M, et al. (2008) Recurrent gross mutations of the PTEN tumor suppressor gene in breast cancers with deficient DSB repair. *Nat Genet* 40: 102–107.
78. Oikawa T (2004) ETS transcription factors: possible targets for cancer therapy. *Cancer Sci* 95: 626–633.
79. Livasy CA, Karaca G, Nanda R, Tretiakova MS, Olopade OI, et al. (2006) Phenotypic evaluation of the basal-like subtype of invasive breast carcinoma. *Mod Pathol* 19: 264–271.
80. Turner NC, Reis-Filho JS (2006) Basal-like breast cancer and the BRCA1 phenotype. *Oncogene* 25: 5846–5853.
81. Sotiriou C, Neo SY, McShane LM, Korn EL, Long PM, et al. (2003) Breast cancer classification and prognosis based on gene expression profiles from a population-based study. *Proc Natl Acad Sci U S A* 100: 10393–10398.
82. Dontu G, El-Ashry D, Wicha MS (2004) Breast cancer, stem/progenitor cells and the estrogen receptor. *Trends Endocrinol Metab* 15: 193–197.
83. Sims AH, Howell A, Howell SJ, Clarke RB (2007) Origins of breast cancer subtypes and therapeutic implications. *Nat Clin Pract Oncol* 4: 516–525.
84. Molyneux G, Regan J, Smalley MJ (2007) Mammary stem cells and breast cancer. *Cell Mol Life Sci* 64: 3248–3260.
85. Polyak K (2007) Breast cancer: origins and evolution. *J Clin Invest* 117: 3155–3163.
86. Sleeman KE, Kendrick H, Robertson D, Isacke CM, Ashworth A, et al. (2007) Dissociation of estrogen receptor expression and in vivo stem cell activity in the mammary gland. *J Cell Biol* 176: 19–26.
87. Wright MH, Calcagno AM, Salcido CD, Carlson MD, Ambudkar SV, et al. (2008) Brca1 breast tumors contain distinct CD44+/CD24- and CD133+ cells with cancer stem cell characteristics. *Breast Cancer Res* 10: R10.
88. Ince TA, Richardson AL, Bell GW, Saitoh M, Godar S, et al. (2007) Transformation of different human breast epithelial cell types leads to distinct tumor phenotypes. *Cancer Cell* 12: 160–170.
89. Richardson C, Stark JM, Ommundsen M, Jasim M (2004) Rad51 overexpression promotes alternative double-strand break repair pathways and genome instability. *Oncogene* 23: 546–553.
90. Kao J, Pollack JR (2006) RNA interference-based functional dissection of the 17q12 amplicon in breast cancer reveals contribution of coamplified genes. *Genes Chromosomes Cancer* 45: 761–769.
91. Streicher KL, Yang ZQ, Draghici S, Ethier SP (2007) Transforming function of the LSM1 oncogene in human breast cancers with the 8p11–12 amplicon. *Oncogene* 26: 2104–2114.
92. Hannon GJ, Rossi JJ (2004) Unlocking the potential of the human genome with RNA interference. *Nature* 431: 371–378.
93. Silva JM, Marran K, Parker JS, Silva J, Golding M, et al. (2008) Profiling essential genes in human mammary cells by multiplex RNAi screening. *Science* 319: 617–620.
94. Hollestelle A, Elstrodt F, Nagel JH, Kallemeijn WW, Schutte M (2007) Phosphatidylinositol-3-OH kinase or RAS pathway mutations in human breast cancer cell lines. *Mol Cancer Res* 5: 195–201.
95. Stemke-Hale K, Gonzalez-Angulo AM, Lluch A, Neve RM, Kuo WL, et al. (2008) An integrative genomic and proteomic analysis of PIK3CA, PTEN, and AKT mutations in breast cancer. *Cancer Res* 68: 6084–6091.
96. Der SD, Zhou A, Williams BR, Silverman RH (1998) Identification of genes differentially regulated by interferon alpha, beta, or gamma using oligonucleotide arrays. *Proc Natl Acad Sci U S A* 95: 15623–15628.
97. Radaeva S, Jaruga B, Hong F, Kim WH, Fan S, et al. (2002) Interferon-alpha activates multiple STAT signals and down-regulates c-Met in primary human hepatocytes. *Gastroenterology* 122: 1020–1034.
98. Jechlinger M, Grunert S, Tamir IH, Janda E, Ludemann S, et al. (2003) Expression profiling of epithelial plasticity in tumor progression. *Oncogene* 22: 7155–7169.
99. Zhang HT, Gorn M, Smith K, Graham AP, Lau KK, et al. (1999) Transcriptional profiling of human microvascular endothelial cells in the proliferative and quiescent state using cDNA arrays. *Angiogenesis* 3: 211–219.
100. Dorsey JF, Cunnick JM, Mane SM, Wu J (2002) Regulation of the Erk2-Elk1 signaling pathway and megakaryocytic differentiation of Bcr-Abl(+) K562 leukemic cells by Gab2. *Blood* 99: 1388–1397.
101. Lindvall C, Hou M, Komurasaki T, Zheng C, Henriksson M, et al. (2003) Molecular characterization of human telomerase reverse transcriptase-immortalized human fibroblasts by gene expression profiling: activation of the epiregulin gene. *Cancer Res* 63: 1743–1747.
102. Hinata K, Gervin AM, Jennifer Zhang Y, Khavari PA (2003) Divergent gene regulation and growth effects by NF-kappa B in epithelial and mesenchymal cells of human skin. *Oncogene* 22: 1955–1964.